Universität Stuttgart

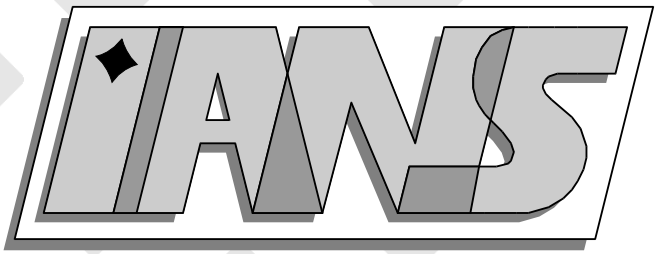

Numerical simulation of linear models for piezoelectric stack actuators

Winfried Geis

Berichte aus dem Institut für Angewandte Analysis und Numerische Simulation

Preprint 2005/007

Universität Stuttgart

Numerical simulation of linear models for piezoelectric stack actuators

Winfried Geis

Berichte aus dem Institut für Angewandte Analysis und Numerische Simulation

Preprint 2005/007

Institut für Angewandte Analysis und Numerische Simulation (IANS)
Fakultät Mathematik und Physik
Fachbereich Mathematik
Pfaffenwaldring 57
D-70 569 Stuttgart

E-Mail: ians-preprints@mathematik.uni-stuttgart.de
WWW: http://preprints.ians.uni-stuttgart.de

ISSN **1611-4176**

Contents

1 Introduction

Piezoelectric stack actuators play an increasing role in technical applications, especially when high generative forces together with short response times are demanded. One example is the application of co-fired multi-layer stack actuators in the injection valves of Diesel engines (see figure 1). To reduce costs and waste, the design of the stack has to be optimised with the

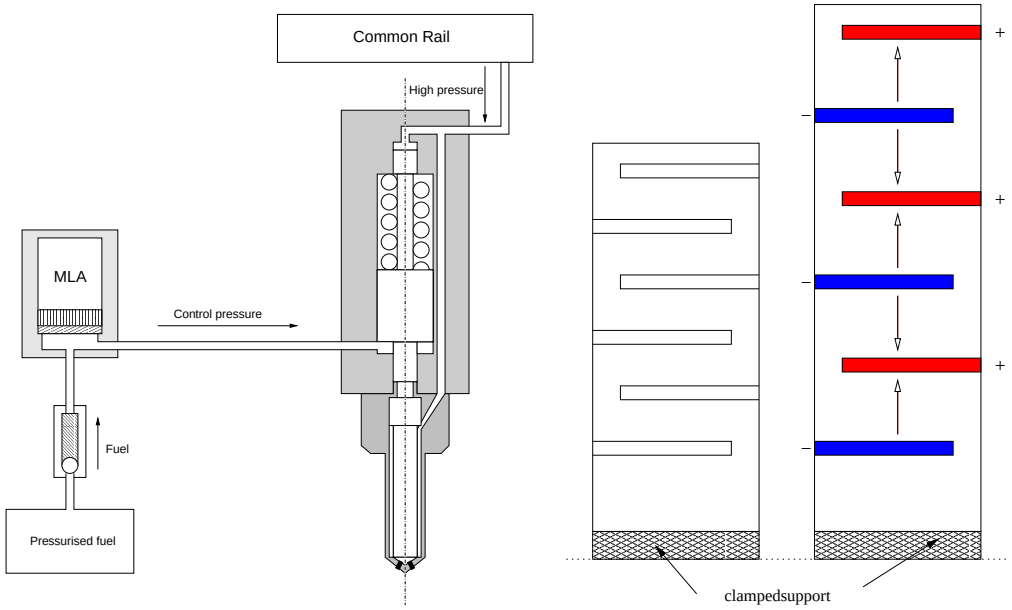

(a) Scheme of an injection nozzle of a common rail engine [10]. The MLA is arranged inside an earthed metal vessel.

(b) Mechanical dilatation of a clamped MLA (cross section) due to an applied voltage.

Figure 1: Multilayer actuator in an injection unit.

help of numerical simulations. Hereby it is basically to determine the deformation and stress singularities.

In this paper, the composite of alternating poled piezoelectric ceramic plates and interdigitated electrodes is modelled as a multi-field-problem for the electric potential field Φ_C and the elastic displacement fields $\underline{\mathbf{u}}_C$ and $\underline{\mathbf{u}}_M$ (C and M denote restrictions to the ceramic or metal sub-domain, respectively). The hysteresis effects in piezoelectric materials are relatively small in brittle ceramics such as PZT-4 which is used e.g. in stack actuators for injection units. Under the assumption that hysteresis effects are neglectable and the stroke of the actuator is small, linear constitutive relations apply for both materials: the piezoelectric ceramic (PZT-4, Barium-Titanate) and the metal alloy (AgPd). The linear constitutive relations of piezoelasticity (at constant temperature) which trace back to W. Voigt [24] couple the equations of linear elasticity with Maxwell's equations:

$$\sigma_{ij} = C_{ijkl}\gamma_{kl} - e_{mij}E_m, \tag{1.1}$$

$$D_n = e_{nij}\gamma_{ij} + \varepsilon_{mn}E_m, \tag{1.2}$$

where $\underline{\underline{\boldsymbol{\gamma}}}$ denotes the strain, $\underline{\underline{\boldsymbol{\sigma}}}$ the stress, $\underline{\boldsymbol{E}}$ the electric vector field and $\underline{\boldsymbol{D}}$ the electric displacement. $\underline{\boldsymbol{E}}$ is assumed to be curl-free, that means, that the influence of the magnetic field is neglected. This assumption is reasonable for a wide range of piezoelectric ceramics (also PZT-4), where the magnetic permeability matrix vanishes. For a description of the general model considering the full Maxwell equations, see [14].
Thus in the metal domain, linear elastic behaviour is assumed:

$$\sigma_{ij} = C_{ijkl}\gamma_{kl}. \tag{1.3}$$

Inserting the equations (1.1)-(1.3) into the equilibrium equations in the ceramic and the metal and applying Gauss' divergence law gives a force balance equation system of time-dependent second order partial differential equations. The assumption of a time-harmonic displacement field $\underline{\mathbf{u}}$ and potential field Φ reduces the force-balance equations to a Helmholtz-type system, which includes also the stationary equations as a special case.
The first part of the paper concentrates on the analysis of mathematical models: appropriate boundary and transmission conditions are derived and weak formulations in appropriate Sobolev spaces are given. Existence and uniqueness results will be presented especially in the time-harmonic case.
The second part focuses on the numerical simulation of the models introduced in the first part. As numerical simulations of the stationary model will show, the corresponding discrete problem (FEM) reacts strongly on small changes in the material parameters and the aspect ratio of the electrodes. A further effect which can be observed in the simulation is the absorption process of stress singularities in zones near corners. Here, the piezoelectric property of the ceramic has a "healing effect" with respect to stress singularities. The enhancement of the model by the influence of exciting voltage frequencies additionally provides information about the distribution of the devices' resonance frequencies.
The numerical computation of the FEM solution provides basically two main difficulties. On the one hand, the thin electrode layer structure requires an increased number of elements although the geometry and the arrangement of the electrodes in the stack actuator is quite simple. On the other hand one has to cope with material parameters of different orders of magnitude and changing polarisation directions due to the fabrication process.
Problems due to the geometry can be overcome by simplified models [7], which are obtained by an asymptotic procedure. However as well preconditioners as solvers have to be adapted to the material parameters that occur in the resulting linear multi-field problem.
Thus the second part has the following main objectives: The numerical investigation

- of the fields in the stationary model for different geometries,
- of the influence of exciting voltage frequencies on the functionality of the actuator and
- of the simplified (asymptotic) model.

2 Model problems and constitutive equations

In this paper, we consider the 2D version of models for co-fired actuators, based on the models introduced in [6] (full model) and [7] (simplified asymptotic model).

2.1 2D-models for piezoelectric stack actuators (with electrodes)

The now following time-dependent multi-structure multi-field model will serve as a basis for the two special cases: the stationary problem and the steady oscillating problem, which have been simulated for different structural and geometrical settings (see section 4). The reduction to a 2D model is obtained by a plane strain assumption (see e.g. [6], [17]).

Time-dependent model Due to symmetries in the elasticity tensors $\underline{\underline{\underline{\underline{\boldsymbol{C}}}}}_C$, the piezoelectric tensor $\underline{\underline{\underline{\boldsymbol{e}}}}$ and the permittivity tensor $\underline{\underline{\boldsymbol{\varepsilon}}}$, the equations (1.1) and (1.2) can be written in two-index notation (Voigt mapping):

$$\underline{\boldsymbol{\sigma}}_C\left(\underline{\mathbf{u}}_C, \Phi_C\right) = \underline{\underline{\boldsymbol{C}}}_C \mathcal{D}\underline{\mathbf{u}}_C + \underline{\underline{\underline{\boldsymbol{e}}}} \nabla\Phi_C \quad \text{in } \Omega_C, \tag{2.1}$$

$$\underline{\boldsymbol{D}}\left(\underline{\mathbf{u}}_C, \Phi_C\right) = \underline{\underline{\underline{\boldsymbol{e}}}} \mathcal{D}\underline{\mathbf{u}}_C - \underline{\underline{\boldsymbol{\varepsilon}}} \nabla\Phi_C \quad \text{in } \Omega_C, \tag{2.2}$$

with the matrix differential operator

$$\mathcal{D} = \begin{pmatrix} \partial_1 & 0 & \partial_3 \\ 0 & \partial_3 & \partial_1 \end{pmatrix}^\top$$

and

$$\underline{\underline{\boldsymbol{C}}}_C = \begin{pmatrix} c_{11} & c_{13} & 0 \\ c_{13} & c_{33} & 0 \\ 0 & 0 & c_{44} \end{pmatrix}, \quad \underline{\underline{\underline{\boldsymbol{e}}}} = \begin{pmatrix} 0 & 0 & e_{15} \\ e_{31} & e_{31} & 0 \end{pmatrix}, \quad \underline{\underline{\boldsymbol{\varepsilon}}} = \begin{pmatrix} \varepsilon_{11} & 0 \\ 0 & \varepsilon_{33} \end{pmatrix}.$$

Note that the assumption, that the electric vector field $\underline{\boldsymbol{E}}$ is curl-free and thus $\underline{\boldsymbol{E}} = -\nabla\Phi$ has already been inserted into equations (2.1) and (2.2). Analogously, Hooke's law which should hold in the metal occupied domain Ω_M reads:

$$\underline{\boldsymbol{\sigma}}_M\left(\underline{\mathbf{u}}_M\right) = \underline{\underline{\boldsymbol{C}}}_M \mathcal{D}\underline{\mathbf{u}}_M \quad \text{in } \Omega_M, \tag{2.3}$$

with

$$\underline{\underline{\boldsymbol{C}}}_M = \begin{pmatrix} \lambda + 2\mu & \lambda & 0 \\ \lambda & \lambda + 2\mu & 0 \\ 0 & 0 & \mu \end{pmatrix}.$$

Inserting the stresses $\underline{\boldsymbol{\sigma}}_C$ (2.1) and $\underline{\boldsymbol{\sigma}}_M$ (2.3) into the equation of motion and assuming absence of volume forces, that means: no influence of weight and heat, it follows:

$$\begin{aligned} \rho_C \ddot{\underline{\mathbf{u}}}_C - \operatorname{Div} \underline{\boldsymbol{\sigma}}_C\left(\underline{\mathbf{u}}_C, \Phi_C\right) &= \underline{\mathbf{0}} \quad \text{in } \Omega_C \\ \rho_M \ddot{\underline{\mathbf{u}}}_M - \operatorname{Div} \underline{\boldsymbol{\sigma}}_M\left(\underline{\mathbf{u}}_M\right) &= \underline{\mathbf{0}} \quad \text{in } \Omega_M, \end{aligned}$$

where ρ denotes the mass density. Thus with $\operatorname{Div} = \mathcal{D}^\top$, the force balance equation system reads:

System of partial differential equations

$$\rho\ddot{\underline{\mathbf{u}}}_C - \mathcal{D}^\top \underline{\underline{\boldsymbol{C}}}_C \mathcal{D}\underline{\mathbf{u}}_C - \mathcal{D}^\top \underline{\underline{\underline{\boldsymbol{e}}}}^\top \nabla\Phi_C = \underline{\mathbf{0}} \qquad \text{in } \Omega_C, \tag{2.4}$$

$$-\operatorname{div}\left(-\underline{\underline{\underline{\boldsymbol{e}}}} \mathcal{D}\underline{\mathbf{u}}_C + \underline{\underline{\boldsymbol{\varepsilon}}} \nabla\Phi_C\right) = 0 \qquad \text{in } \Omega_C, \tag{2.5}$$

$$\rho\ddot{\underline{\mathbf{u}}}_M - \mathcal{D}^T \underline{\underline{\boldsymbol{C}}}_M \mathcal{D}\underline{\mathbf{u}}_M = \underline{\mathbf{0}} \qquad \text{in } \Omega_M. \tag{2.6}$$

To simplify the notation, the force balance equation system (2.4)-(2.5) can be interpreted as a force balance equation to an extended Hooke's law

$$\partial_{tt}\underline{\mathbf{u}} - \underline{\underline{\boldsymbol{B}}}^{\top}\underline{\underline{\boldsymbol{A}}}\,\underline{\underline{\boldsymbol{B}}}\,\underline{\mathbf{U}} = \underline{\mathbf{0}},$$

where $\underline{\underline{\boldsymbol{B}}}$ is the differential operator:

$$\underline{\underline{\boldsymbol{B}}} = \begin{pmatrix} \mathcal{D}^{\top} & \underline{\mathbf{0}} \\ \underline{\mathbf{0}} & -\nabla_{1,3}^{\top} \end{pmatrix} = \begin{pmatrix} \partial_1 & 0 & \partial_3 & 0 & 0 \\ 0 & \partial_3 & \partial_1 & 0 & 0 \\ 0 & 0 & 0 & -\partial_1 & -\partial_3 \end{pmatrix}^{\top}$$

and $\underline{\mathbf{U}} = \begin{pmatrix} \underline{\mathbf{u}} \\ \phi \end{pmatrix}$ denotes the extended displacement field vector. $\underline{\underline{\boldsymbol{A}}}$ (with its restrictions $\underline{\underline{\boldsymbol{A}}}_C$ to Ω_C and $\underline{\underline{\boldsymbol{A}}}_M$ to Ω_M) is the full material matrix describing the elastic, dielectric and piezo-elastic behaviour of the ceramic and metal, respectively:

$$\underline{\underline{\boldsymbol{A}}}_C = \begin{pmatrix} \underline{\underline{\boldsymbol{C}}}_C & -\underline{\underline{\boldsymbol{e}}}^{\top} \\ \underline{\underline{\boldsymbol{e}}} & \underline{\underline{\boldsymbol{\varepsilon}}} \end{pmatrix} = \begin{pmatrix} c_{11} & c_{13} & 0 & 0 & -e_{31} \\ c_{13} & c_{33} & 0 & 0 & -e_{33} \\ 0 & 0 & c_{44} & -e_{15} & 0 \\ 0 & 0 & e_{15} & \varepsilon_{11} & 0 \\ e_{31} & e_{31} & 0 & 0 & \varepsilon_{33} \end{pmatrix},$$

$$\underline{\underline{\boldsymbol{A}}}_M = \begin{pmatrix} \underline{\underline{\boldsymbol{C}}}_M & \underline{\mathbf{0}} \\ \underline{\mathbf{0}} & \underline{\mathbf{0}} \end{pmatrix} = \begin{pmatrix} \lambda{+}2\mu & \lambda & 0 & & \\ \lambda & \lambda{+}2\mu & 0 & \underline{\mathbf{0}} & \\ 0 & 0 & \mu & & \\ & \underline{\mathbf{0}} & & \underline{\mathbf{0}} & \end{pmatrix}. \tag{2.7}$$

Figure 2 shows the simplest possible geometry of a stack actuator. According to the notation

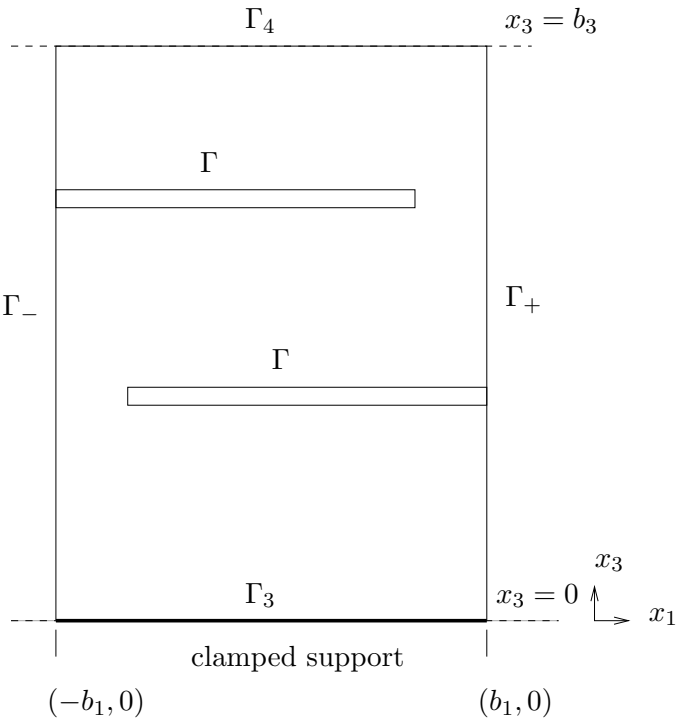

Γ_- $\quad x_1 = -b_1$, $0 \le x_3 \le b_3$

Γ_+ $\quad x_1 = +b_1$, $0 \le x_3 \le b_3$

Γ_3 $\quad -b_1 \le x_1 \le b_1$, $x_3 = 0$,

Γ_4 $\quad -b_1 \le x_1 \le b_1$, $x_3 = b_3$

Figure 2: Boundaries and interfaces of a stack actuator of width $2b_1$, measured in x_1-direction and height b_3.

in figure 2, we assume that the actuator is clamped on the boundary Γ_3. The set of interfaces between metal electrodes Ω_M and the ceramic matrix Ω_C is denoted as $\Gamma = \partial\Omega_M \cap \partial\Omega_C$. Γ_- and the electrodes connected with this boundary (Γ_{cathode}) are on the same potential $\Phi_a^-(t)$ (not dependent on the space variable). Analogously, the applied voltage on Γ_+ and all connected electrodes (Γ_{anode}) is $\Phi_a^+(t)$. Under the assumption that no other outer forces except the electrical loading appear, the normal stress vanishes on Γ_4, Γ_- and Γ_+. Thus the resulting problem, based on the linear Voigt model [24] in Ω_C and the elastic wave equation in Ω_M reads:
Find the displacement $\underline{\mathbf{u}}$ and the electric potential field Φ such that the force balance equations (2.4)- (2.6) are satisfied and the following boundary and transmission conditions hold:
Boundary conditions

$$\boldsymbol{\sigma}_{C_n}(\underline{\mathbf{u}}_C, \Phi_C) = \underline{\mathbf{0}} \qquad \text{on } (\Gamma_\mp \cup \Gamma_4) \cap \partial\Omega_C, \tag{2.8}$$
$$\Phi_C = \Phi_a \qquad \text{on } \Gamma_\mp \cup \Gamma, \tag{2.9}$$
$$\boldsymbol{\sigma}_{M_n}(\underline{\mathbf{u}}_M) = \underline{\mathbf{0}} \qquad \text{on } \Gamma_\mp \cap \partial\Omega_M, \tag{2.10}$$
$$\underline{\mathbf{u}}_C = \underline{\mathbf{0}} \qquad \text{on } \Gamma_3, \tag{2.11}$$
$$D_{C_n}(\underline{\mathbf{u}}_C, \Phi_C) = 0 \qquad \text{on } (\Gamma_3 \cup \Gamma_4) \cap \partial\Omega_C, \tag{2.12}$$

where

$$\Phi_a(\underline{\boldsymbol{x}}, t) := \begin{cases} \Phi_a^-(t) & \text{for } x \in \Gamma_{\text{cathode}}, \\ \Phi_a^+(t) & \text{for } x \in \Gamma_{\text{anode}}, \end{cases} \tag{2.13}$$

Transmission conditions

$$\underline{\mathbf{u}}_C = \underline{\mathbf{u}}_M \qquad \text{on } \Gamma, \tag{2.14}$$
$$\boldsymbol{\sigma}_{C_n}(\underline{\mathbf{u}}_C, \Phi_C) = \boldsymbol{\sigma}_{M_n}(\underline{\mathbf{u}}_M) \qquad \text{on } \Gamma. \tag{2.15}$$

Initial conditions complete this model.

Here, the index n in $\underline{\boldsymbol{\sigma}}_{C_n}$ and $\underline{\boldsymbol{\sigma}}_{M_n}$ denotes the normal stress. D_{C_n} is the normal component of the electric displacement D.
To derive the so called steady-oscillation and the stationary case from the system (2.4)-(2.6) of partial differential equations, it is assumed, that the fields $\underline{\mathbf{u}}(\underline{\boldsymbol{x}}, t)$ and $\Phi(\underline{\boldsymbol{x}}, t)$ are of the form

$$\underline{\mathbf{u}}(\underline{\boldsymbol{x}}, t) = \underline{\boldsymbol{u}}(\underline{\boldsymbol{x}})\, e^{\tau t} \tag{2.16}$$
$$\Phi(\underline{\boldsymbol{x}}, t) = \Phi(\underline{\boldsymbol{x}})\, e^{\tau t} \tag{2.17}$$

with the amplitudes $\underline{\boldsymbol{u}}(\underline{\boldsymbol{x}})$ and $\Phi(\underline{\boldsymbol{x}})$ and $\tau := s + i\omega$ (pseudo-oscillating Ansatz, see [23]).

Stationary model ($\tau = 0$) It is assumed, that τ appearing in the exponent of the multiplier $e^{\tau t}$ in (2.16) and (2.17) is zero. This means that the sought-after $\underline{\boldsymbol{u}}$ and Φ do not depend on the time-variable. Therefore, the original time-dependent problem simplifies (see [6]) to:
Find the displacement field $\underline{\boldsymbol{u}}(\underline{\boldsymbol{x}})$ and the electric potential field $\Phi(\underline{\boldsymbol{x}})$ such that:

System of partial differential equations

$$-\mathcal{D}^\top \underline{\underline{\boldsymbol{C}}}_C \mathcal{D}\underline{\boldsymbol{u}}_C - \mathcal{D}^\top \underline{\underline{\boldsymbol{e}}}^\top \nabla\Phi_C = \underline{\mathbf{0}} \qquad \text{in } \Omega_C, \tag{2.18}$$

$$-\operatorname{div}\left(-\underline{\underline{\boldsymbol{e}}}\,\mathcal{D}\underline{\boldsymbol{u}}_C + \underline{\underline{\boldsymbol{\varepsilon}}}\,\nabla\Phi_C\right) = 0 \qquad \text{in } \Omega_C, \tag{2.19}$$

$$-\mathcal{D}^T \underline{\underline{\boldsymbol{C}}}_M \mathcal{D}\underline{\boldsymbol{u}}_M = \underline{\mathbf{0}} \qquad \text{in } \Omega_M. \tag{2.20}$$

Boundary conditions

$$\boldsymbol{\sigma}_{C_n}(\underline{\boldsymbol{u}}_C, \Phi_C) = \underline{\mathbf{0}} \qquad \text{on } (\Gamma_\mp \cup \Gamma_4) \cap \partial\Omega_C, \tag{2.21}$$

$$\Phi_C = \mp\Phi_a \qquad \text{on } \Gamma_\mp \cup \Gamma, \tag{2.22}$$

$$\boldsymbol{\sigma}_{M_n}(\underline{\boldsymbol{u}}_M) = \underline{\mathbf{0}} \qquad \text{on } \Gamma_\mp \cap \partial\Omega_M, \tag{2.23}$$

$$\underline{\boldsymbol{u}}_C = \underline{\mathbf{0}} \qquad \text{on } \Gamma_3, \tag{2.24}$$

$$D_{C_n}(\underline{\boldsymbol{u}}_C, \Phi_C) = 0 \qquad \text{on } (\Gamma_3 \cup \Gamma_4) \cap \partial\Omega_C, \tag{2.25}$$

where Φ_a is constant.

Transmission conditions

$$\underline{\boldsymbol{u}}_C = \underline{\boldsymbol{u}}_M \qquad \text{on } \Gamma, \tag{2.26}$$

$$\boldsymbol{\sigma}_{C_n}(\underline{\boldsymbol{u}}_C, \Phi_C) = \boldsymbol{\sigma}_{M_n}(\underline{\boldsymbol{u}}_M) \qquad \text{on } \Gamma. \tag{2.27}$$

To compute weak (finite element) solutions $\underline{\boldsymbol{U}} = \left(\begin{smallmatrix}\boldsymbol{u}\\ \Phi\end{smallmatrix}\right)$, a smooth continuation $\underline{\boldsymbol{W}} := \left(\begin{smallmatrix}\mathbf{0}\\ \hat{\Phi}\end{smallmatrix}\right) \in \left[\mathsf{H}^1(\Omega)\right]^3$ of the non-homogeneous electric Dirichlet data is introduced and the boundary-transmission problem (2.18)-(2.27) is reformulated in the Sobolev space $\mathcal{V}$, with

$$\left[\mathsf{H}^1(\Omega)\right]^3 \supseteq \mathcal{V} := \left\{ \underline{\boldsymbol{V}} = \left(\begin{smallmatrix}\boldsymbol{v}\\ \Psi\end{smallmatrix}\right) \in \left[\mathsf{H}^1(\Omega)\right]^3, r_{\big|\Gamma^D_{C,m}} \underline{\boldsymbol{v}}_C = \underline{\mathbf{0}} \text{ and } r_{\big|\Gamma^D_{C,e}} \Psi_C = 0 \right\}. \tag{2.28}$$

The upper index D of the boundary parts $\Gamma^{\cdot}_{C,\cdot}$ denotes Dirichlet conditions, the lower index e refers to the electric potential field and m to the displacement field.

Lemma 2.1. *Let $\underline{\boldsymbol{W}}$ be a smooth continuation of the non-homogeneous Dirichlet data (2.22) and $\underline{\boldsymbol{U}}^0 \in \mathcal{V}$ such that $\underline{\boldsymbol{U}}^0 := \underline{\boldsymbol{U}} - \underline{\boldsymbol{W}}$. Then for every $\underline{\boldsymbol{V}} \in \mathcal{V}$, the weak formulation of the boundary-transmission problem (2.18)-(2.27) reads: Find $\underline{\boldsymbol{U}}^0 \in \mathcal{V}$ such that*

$$a\left(\underline{\boldsymbol{U}}^0, \underline{\boldsymbol{V}}\right) = a_C\left(\underline{\boldsymbol{U}}^0_C, \underline{\boldsymbol{V}}_C\right) + a_M\left(\underline{\boldsymbol{U}}^0_M, \underline{\boldsymbol{V}}_M\right) = -a_C\left(\underline{\boldsymbol{W}}, \underline{\boldsymbol{V}}\right) \tag{2.29}$$

holds for all $\underline{\boldsymbol{V}} \in \mathcal{V}$, where

$$a_C\left(\underline{\boldsymbol{U}}^0_C, \underline{\boldsymbol{V}}_C\right) := \int_{\Omega_C} \underline{\underline{\boldsymbol{A}}}_C \underline{\underline{\boldsymbol{B}}}\, \underline{\boldsymbol{U}}^0_C \cdot \underline{\underline{\boldsymbol{B}}}\, \underline{\boldsymbol{V}}_C \,\mathrm{d}\underline{\boldsymbol{x}}, \tag{2.30}$$

$$a_M\left(\underline{\boldsymbol{U}}^0_M, \underline{\boldsymbol{V}}_M\right) := \int_{\Omega_M} \underline{\underline{\boldsymbol{C}}}_M \mathcal{D}\underline{\boldsymbol{u}}^0_M \cdot \mathcal{D}\underline{\boldsymbol{v}}_M \,\mathrm{d}\underline{\boldsymbol{x}}. \tag{2.31}$$

Proof. See [6], lemma 5.1. □

Theorem 2.1. *Let $\mathfrak{A} : \mathcal{V} \to \mathcal{V}'$ be the operator, defined by the bilinear forms (2.30)-(2.31): $\langle \mathfrak{A}\underline{\boldsymbol{U}}^{\mathbf{0}}, \underline{\boldsymbol{V}} \rangle := a\left(\underline{\boldsymbol{U}}^{\mathbf{0}}, \underline{\boldsymbol{V}}\right) = a_C\left(\underline{\boldsymbol{U}}^0_C, \underline{\boldsymbol{V}}_C\right) + a_M\left(\underline{\boldsymbol{U}}^0_M, \underline{\boldsymbol{V}}_M\right)$. Then $\mathfrak{A}$ satisfies conditions of the Lax-Milgram lemma and thus an unique weak solution $\underline{\boldsymbol{U}}^0$ of (2.29) (and thus $\underline{\boldsymbol{U}}$) exists.*

Proof. This theorem is a special case of Theorem 5.1 in [6]. □

Steady oscillations (Helmholtz-type model) To derive the steady oscillation formulation, one assumes $\tau = \imath\omega_l$, such that $\underline{\mathbf{u}}_C$, $\underline{\mathbf{u}}_M$ and Φ are of the form $\underline{\mathbf{u}}_C := e^{i\omega_0 t}$, $\Phi_C := e^{i\omega_1 t}$ and $\underline{\mathbf{u}}_M = e^{i\omega_2 t}$. Due to the strong coupling, expressed by the transmission conditions (2.14) and (2.15), it follows the equality of ω_i. Therefore we simply write $\underline{\mathbf{u}} = e^{i\omega t}\underline{\boldsymbol{u}}(\underline{\boldsymbol{x}})$ and $\Phi = e^{i\omega t}\Phi(\underline{\boldsymbol{x}})$. Inserting this Ansatz into (2.4)-(2.15) results in a system for the amplitudes $\underline{\boldsymbol{u}}(\underline{\boldsymbol{x}})$ and $\Phi(\underline{\boldsymbol{x}})$. The steady-oscillating problem reads:
Find the displacement $\underline{\boldsymbol{u}}(\underline{\boldsymbol{x}})$ and the electric potential field $\Phi(\underline{\boldsymbol{x}})$ such that:

System of partial differential equations

$$-\rho_C\omega^2\underline{\boldsymbol{u}}_C - \mathcal{D}^\top\underline{\underline{\boldsymbol{C}}}_C\mathcal{D}\underline{\boldsymbol{u}}_C - \mathcal{D}^\top\underline{\underline{\boldsymbol{e}}}^\top\nabla\Phi_C = \underline{\mathbf{0}} \qquad \text{in } \Omega_C, \tag{2.32}$$

$$-\operatorname{div}\left(-\underline{\underline{\boldsymbol{e}}}\,\mathcal{D}\underline{\boldsymbol{u}}_C + \underline{\underline{\boldsymbol{\varepsilon}}}\,\nabla\Phi_C\right) = 0 \qquad \text{in } \Omega_C, \tag{2.33}$$

$$-\rho_M\omega^2\underline{\boldsymbol{u}}_M - \mathcal{D}^T\underline{\underline{\boldsymbol{C}}}_M\mathcal{D}\underline{\boldsymbol{u}}_M = \underline{\mathbf{0}} \qquad \text{in } \Omega_M. \tag{2.34}$$

Boundary conditions

$$\boldsymbol{\sigma}_{C_n}(\underline{\boldsymbol{u}}_C, \Phi_C) = \underline{\mathbf{0}} \qquad \text{on } (\Gamma_\mp \cup \Gamma_4) \cap \partial\Omega_C, \tag{2.35}$$

$$\Phi_C = \mp\Phi_a \qquad \text{on } \Gamma_\mp \cup \Gamma, \tag{2.36}$$

$$\boldsymbol{\sigma}_{M_n}(\underline{\boldsymbol{u}}_M) = \underline{\mathbf{0}} \qquad \text{on } \Gamma_\mp \cap \partial\Omega_M, \tag{2.37}$$

$$\underline{\boldsymbol{u}}_C = \underline{\mathbf{0}} \qquad \text{on } \Gamma_3, \tag{2.38}$$

$$D_{C_n}(\underline{\boldsymbol{u}}_C, \Phi_C) = 0 \qquad \text{on } (\Gamma_3 \cup \Gamma_4) \cap \partial\Omega_C, \tag{2.39}$$

where Φ_a is constant.

Transmission conditions

$$\underline{\boldsymbol{u}}_C = \underline{\boldsymbol{u}}_M \qquad \text{on } \Gamma, \tag{2.40}$$

$$\boldsymbol{\sigma}_{C_n}(\underline{\boldsymbol{u}}_C, \Phi_C) = \boldsymbol{\sigma}_{M_n}(\underline{\boldsymbol{u}}_M) \qquad \text{on } \Gamma. \tag{2.41}$$

The weak formulation in the space $\mathcal{V}$, introduced in (2.28) reads:

Lemma 2.2. *Let $\underline{\boldsymbol{W}} \in \left[\mathsf{H}^1(\Omega)\right]^3$ be a smooth continuation of the non-homogeneous Dirichlet data of $\underline{\boldsymbol{U}}$ and $\underline{\boldsymbol{U}}^0 \in \mathcal{V}$ such that $\underline{\boldsymbol{U}}^0 := \underline{\boldsymbol{U}} - \underline{\boldsymbol{W}}$. Then for every $\underline{\boldsymbol{V}} \in \mathcal{V}$, the weak formulation of the boundary-transmission problem (2.32)-(2.41) reads: Find $\underline{\boldsymbol{U}}^0 \in \mathcal{V}$ such that*

$$a_{so}\left(\underline{\boldsymbol{U}}^0, \underline{\boldsymbol{V}}\right) = a_{C,so}\left(\underline{\boldsymbol{U}}^0_C, \underline{\boldsymbol{V}}_C\right) + a_{M,so}\left(\underline{\boldsymbol{U}}^0_M, \underline{\boldsymbol{V}}_M\right) = -a_{C,so}\left(\underline{\boldsymbol{W}}, \underline{\boldsymbol{V}}\right) \tag{2.42}$$

holds for all $\underline{\boldsymbol{V}} \in \mathcal{V}$, where

$$a_{C,so}\left(\underline{\boldsymbol{U}}^0_C, \underline{\boldsymbol{V}}_C\right) := -\rho_C\omega^2\int_{\Omega_C}\underline{\boldsymbol{u}}^0_C\cdot\underline{\boldsymbol{v}}_C\,\mathrm{d}\underline{\boldsymbol{x}} + \int_{\Omega_C}\underline{\underline{\boldsymbol{A}}}_C\underline{\underline{\boldsymbol{B}}}\,\underline{\boldsymbol{U}}^0_C\cdot\underline{\underline{\boldsymbol{B}}}\,\underline{\boldsymbol{V}}_C\,\mathrm{d}\underline{\boldsymbol{x}}, \tag{2.43}$$

$$a_{M,so}\left(\underline{\boldsymbol{U}}^0_M, \underline{\boldsymbol{V}}_M\right) := -\rho_M\omega^2\int_{\Omega_M}\underline{\boldsymbol{u}}^0_M\cdot\underline{\boldsymbol{v}}_M\,\mathrm{d}\underline{\boldsymbol{x}} + \int_{\Omega_M}\underline{\underline{\boldsymbol{C}}}_M\mathcal{D}\underline{\boldsymbol{u}}^0_M\cdot\mathcal{D}\underline{\boldsymbol{v}}_M\,\mathrm{d}\underline{\boldsymbol{x}}. \tag{2.44}$$

Note, that $a_{C,so}$ and $a_{M,so}$ are restrictions of a_{so} to the sub-domains Ω_C and Ω_M. The index *so* denotes the steady oscillations case.

Proof. Due to (2.32)-(2.34), it holds

$$\begin{aligned}\int_\Omega \left(-\rho\omega^2 - \underline{\underline{\boldsymbol{B}}}^\top \underline{\underline{\boldsymbol{A}}}\,\underline{\underline{\boldsymbol{B}}}\,\underline{\boldsymbol{U}}\right)\cdot V\,\mathrm{d}\underline{\boldsymbol{x}} &= \int_\Omega -\rho\omega^2 \underline{\boldsymbol{u}}^{\,0}\cdot\underline{\boldsymbol{v}} \\ &\quad - \int_\Omega \underline{\underline{\boldsymbol{B}}}^\top \underline{\underline{\boldsymbol{A}}}\,\underline{\underline{\boldsymbol{B}}}\,\left(\underline{\boldsymbol{W}} + \underline{\boldsymbol{U}}^{\,0}\right)\cdot\underline{\boldsymbol{V}}\,\mathrm{d}\underline{\boldsymbol{x}} \\ -\rho\omega^2\int_\Omega \underline{\boldsymbol{u}}^{\,0}\cdot\underline{\boldsymbol{v}}\,\mathrm{d}\underline{\boldsymbol{x}} + \int_\Omega \underline{\underline{\boldsymbol{A}}}\,\underline{\underline{\boldsymbol{B}}}\,\underline{\boldsymbol{U}}^{\,0}\cdot\underline{\underline{\boldsymbol{B}}}\,\underline{\boldsymbol{V}}\,\mathrm{d}\underline{\boldsymbol{x}} &= \int_\Omega -\rho\omega^2\underline{\boldsymbol{0}}\cdot\underline{\boldsymbol{v}}\,\mathrm{d}\underline{\boldsymbol{x}} - \int_\Omega \underline{\underline{\boldsymbol{A}}}\,\underline{\underline{\boldsymbol{B}}}\,\underline{\boldsymbol{W}}\cdot\underline{\underline{\boldsymbol{B}}}\,\underline{\boldsymbol{V}}\,\mathrm{d}a_{\underline{\boldsymbol{x}}} \\ &\quad + \int_{\partial\Omega} \underline{\underline{\boldsymbol{N}}}^\top \underline{\underline{\boldsymbol{A}}}\,\underline{\underline{\boldsymbol{B}}}\,\underline{\boldsymbol{U}}\cdot\underline{\underline{\boldsymbol{B}}}\,\underline{\boldsymbol{V}}\,\mathrm{d}a_{\underline{\boldsymbol{x}}}.\end{aligned}$$

Inserting the boundary and transmission conditions (2.35)-(2.41), the boundary integral term on the right hand side vanishes and it follows, that

$$a_{so}\left(\underline{\boldsymbol{U}}^{\,0},\underline{\boldsymbol{V}}\right) = -a_{so}\left(\underline{\boldsymbol{W}},\underline{\boldsymbol{V}}\right).$$

□

Theorem 2.2. *Let $\mathfrak{A}_{so}:\mathcal{V}\to\mathcal{V}'$ be the operator, defined by the bilinear forms (2.43)-(2.44): $\left\langle \mathfrak{A}_{so}\underline{\boldsymbol{U}}^{\boldsymbol{0}},\underline{\boldsymbol{V}}\right\rangle := a_{so}\left(\underline{\boldsymbol{U}}^{\boldsymbol{0}},\underline{\boldsymbol{V}}\right) = a_{C,so}\left(\underline{\boldsymbol{U}}^{\,0}_{C},\underline{\boldsymbol{V}}_{C}\right) + a_{M,so}\left(\underline{\boldsymbol{U}}^{\,0}_{M},\underline{\boldsymbol{V}}_{M}\right)$. Then $\mathfrak{A}_{so}$ satisfies for small frequencies ω (below the smallest eigenfrequency of the system) the Lax-Milgram conditions and therefore a unique weak solution $\underline{\boldsymbol{U}}^{\,0}$ of (2.29) (and thus $\underline{\boldsymbol{U}}$) exists.*

Proof. To proof the theorem, the Lax-Milgram conditions have to be satisfied, that means

- a_{so} is $\mathcal{V}$-bounded and thus continuous.
- a_{so} is $\mathcal{V}$-elliptic, provided, ω is small (see numerical examples in section 4) and $\underline{\underline{\boldsymbol{C}}}$ and $\underline{\underline{\boldsymbol{\epsilon}}}$ are positive definite (see also [6]).

For simplicity, material tensors and fields are written without any index, if they are related to the whole domain, e.g.

$$\underline{\underline{\boldsymbol{A}}} = \underline{\underline{\boldsymbol{A}}}\left(\underline{\boldsymbol{x}}\right) := \begin{cases}\underline{\underline{\boldsymbol{A}}}_C & \underline{\boldsymbol{x}}\in\Omega_C\\ \underline{\underline{\boldsymbol{A}}}_M & \underline{\boldsymbol{x}}\in\Omega_M.\end{cases}$$

Continuity. Let $\underline{\boldsymbol{U}},\underline{\boldsymbol{V}}\in\mathcal{V}$. Then it follows, that:

$$\begin{aligned}\left|a_{so}\left(\underline{\boldsymbol{U}},\underline{\boldsymbol{V}}\right)\right| &= \left|\int_\Omega -\rho\omega^2\underline{\boldsymbol{u}}\cdot\underline{\boldsymbol{v}}\,\mathrm{d}\underline{\boldsymbol{x}} + \int_\Omega \underline{\underline{\boldsymbol{A}}}\,\underline{\underline{\boldsymbol{B}}}\,\underline{\boldsymbol{U}}\cdot\underline{\underline{\boldsymbol{B}}}\,\underline{\boldsymbol{V}}\,\mathrm{d}\underline{\boldsymbol{x}}\right| \\ &\le \rho\omega^2\left|\int_\Omega \underline{\boldsymbol{u}}\cdot\underline{\boldsymbol{v}}\,\mathrm{d}\underline{\boldsymbol{x}}\right| + \sum_{i=1}^{5}\left|\int_\Omega \left(\underline{\underline{\boldsymbol{A}}}\,\underline{\underline{\boldsymbol{B}}}\,\underline{\boldsymbol{U}}\right)_i\left(\underline{\underline{\boldsymbol{B}}}\,\underline{\boldsymbol{V}}\right)_i\mathrm{d}\underline{\boldsymbol{x}}\right| \\ &\le \rho\omega^2\left\|\underline{\boldsymbol{U}}\right\|_{[L_2(\Omega)]^3}\left\|\underline{\boldsymbol{V}}\right\|_{[L_2(\Omega)]^3} + \max|A_{ij}|\left(\left\|\partial_1 u_1\right\|_{L_2(\Omega)}\left\|\partial_1 v_1\right\|_{L_2(\Omega)}\right. \\ &+ \left\|\partial_3 u_3\right\|_{L_2(\Omega)}\left\|\partial_3 v_3\right\|_{L_2(\Omega)} + \left\|\partial_3 u_1+\partial_1 u_3\right\|_{L_2(\Omega)}\left\|\partial_3 v_1+\partial_1 v_3\right\|_{L_2(\Omega)} \\ &+ \left.\left\|\partial_1\Phi\right\|_{L_2(\Omega)}\left\|\partial_1\Psi\right\|_{L_2(\Omega)} + \left\|\partial_3\Phi\right\|_{L_2(\Omega)}\left\|\partial_3\Psi\right\|_{L_2(\Omega)}\right) \\ &\le \rho\omega^2\left\|\underline{\boldsymbol{U}}\right\|_{\mathcal{V}}\left\|\underline{\boldsymbol{V}}\right\|_{\mathcal{V}} + \max|A_{i,j}|\left\|\underline{\boldsymbol{U}}\right\|_{\mathcal{V}}\left\|\underline{\boldsymbol{V}}\right\|_{\mathcal{V}} \\ &\le \underbrace{\max\left(\rho\omega^2,|A_{i,j}|\right)}_{=:C}\left\|\underline{\boldsymbol{U}}\right\|_{\mathcal{V}}\left\|\underline{\boldsymbol{V}}\right\|_{\mathcal{V}} \qquad (2.45)\end{aligned}$$

$\mathcal{V}$-Ellipticity. Let $\underline{\boldsymbol{E}} = \underline{\boldsymbol{E}}(\Phi)$ denote the electrical vector field and $\underline{\boldsymbol{\gamma}} = \underline{\boldsymbol{\gamma}}(\underline{\boldsymbol{u}})$ the mechanical strain. Due to the block structure of $\underline{\underline{\boldsymbol{A}}}$, a_{so} can be written as

$$\begin{aligned} a_{so}(\underline{\boldsymbol{U}}, \underline{\boldsymbol{U}}) &= \int_\Omega \begin{pmatrix} \underline{\boldsymbol{\gamma}} \\ \underline{\boldsymbol{E}} \end{pmatrix}^\top \begin{pmatrix} \underline{\underline{\boldsymbol{C}}} & -\underline{\underline{\boldsymbol{e}}}^\top \\ \underline{\underline{\boldsymbol{e}}} & \underline{\underline{\boldsymbol{\varepsilon}}} \end{pmatrix} \begin{pmatrix} \underline{\boldsymbol{\gamma}} \\ \underline{\boldsymbol{E}} \end{pmatrix} \mathrm{d}\underline{\boldsymbol{x}} - \int_\Omega \rho\omega^2 \, \underline{\boldsymbol{u}} \cdot \underline{\boldsymbol{v}} \, \mathrm{d}\underline{\boldsymbol{x}} \\ &= \int_\Omega \underline{\boldsymbol{\gamma}}^\top \underline{\underline{\boldsymbol{C}}} \underline{\boldsymbol{\gamma}} + \underline{\boldsymbol{\gamma}}^\top \underline{\underline{\boldsymbol{e}}}^\top \underline{\boldsymbol{E}} - \underline{\boldsymbol{E}}^\top \underline{\underline{\boldsymbol{e}}} \underline{\boldsymbol{\gamma}} + \underline{\boldsymbol{E}}^\top \underline{\underline{\boldsymbol{\varepsilon}}} \underline{\boldsymbol{E}} \, \mathrm{d}\underline{\boldsymbol{x}} - \rho\omega^2 \left\| \underline{\boldsymbol{u}} \right\|^2_{[L_2(\Omega)]^2} \\ &= \int_\Omega \underline{\boldsymbol{\gamma}}^\top \underline{\underline{\boldsymbol{C}}} \underline{\boldsymbol{\gamma}} + \underline{\boldsymbol{E}}^\top \underline{\underline{\boldsymbol{\varepsilon}}} \underline{\boldsymbol{E}} \, \mathrm{d}\underline{\boldsymbol{x}} - \rho\omega^2 \left\| \underline{\boldsymbol{u}} \right\|^2_{[L_2(\Omega)]^2}. \end{aligned} \tag{2.46}$$

Thus $a_{so}(\underline{\boldsymbol{U}}, \underline{\boldsymbol{U}})$ is independent of the piezoelectric tensor $\underline{\underline{\boldsymbol{e}}}$. To simplify the estimate, the mechanical and electrical part of the integral term (2.46) are splitted and estimated separately:

Mechanical part. Let $c_0 := \min\{c_M, c_C\}$, where c_M and c_C are the smallest eigenvalues of $\underline{\underline{\boldsymbol{C}}}_C$ and $\underline{\underline{\boldsymbol{C}}}_M$, respectively. Since the Dirichlet boundary is a non-empty 2D set, one can apply Korn's 2. inequality [1], such that

$$\begin{aligned} \int_\Omega \underline{\boldsymbol{\gamma}}^\top \underline{\underline{\boldsymbol{C}}} \underline{\boldsymbol{\gamma}} \, \mathrm{d}\underline{\boldsymbol{x}} - \rho\omega^2 \left\| \underline{\boldsymbol{u}} \right\|^2_{[L_2(\Omega)]^2} &\geq c_0 \int_\Omega \underline{\boldsymbol{\gamma}}^\top \cdot \underline{\boldsymbol{\gamma}} \, \mathrm{d}\underline{\boldsymbol{x}} - \rho\omega^2 \left\| \underline{\boldsymbol{u}} \right\|^2_{\mathcal{V}} \\ &= c_0 \left\| \underline{\boldsymbol{\gamma}} \right\|^2_{[L_2(\Omega)]^2} - \rho\omega^2 \left\| \underline{\boldsymbol{u}} \right\|^2_{\mathcal{V}} \\ &\overset{\text{Korn}}{\geq} c_{0,\text{Korn}}\left(c_0, \Omega, \Gamma_m^D\right) \left\| \underline{\boldsymbol{u}} \right\|^2_{\mathcal{V}} - \rho\omega^2 \left\| \underline{\boldsymbol{u}} \right\|^2_{\mathcal{V}} \quad \geq c_1 \left\| \underline{\boldsymbol{u}} \right\|^2_{\mathcal{V}} \end{aligned}$$

follows, with $c_1 > 0$ for small ω.

Electrical part. Analogously, one can estimate the electrical part with the help of Friedrichs inequality:

$$\begin{aligned} \int_\Omega \underline{\boldsymbol{E}}^\top \underline{\underline{\boldsymbol{\varepsilon}}} \underline{\boldsymbol{E}} \, \mathrm{d}\underline{\boldsymbol{x}} &= \int_{\Omega_C} \underline{\boldsymbol{E}}_C^\top \underline{\underline{\boldsymbol{\varepsilon}}}_C \underline{\boldsymbol{E}}_C \, \mathrm{d}\underline{\boldsymbol{x}} \\ &\underbrace{\geq \min(\varepsilon_{11}, \varepsilon_{33})}_{=:\varepsilon_0} \int_{\Omega_C} \nabla\Phi \cdot \nabla\Phi \, \mathrm{d}\underline{\boldsymbol{x}} \\ &= \varepsilon_0 \int_\Omega \nabla\Phi \cdot \nabla\Phi \, \mathrm{d}\underline{\boldsymbol{x}} \geq \varepsilon_{0,\text{Friedrichs}}\left(\varepsilon_0, \Omega_C, \Gamma_e^D\right) \left\| \Phi \right\|^2_{\mathcal{V}}. \end{aligned}$$

Thus with the ellipticity constant $\alpha = \min(\varepsilon_{0,\text{Friedrichs}}, c_1)$ follows the assertion. □

Remark 2.1. *More general existence and uniqueness results can be found in [14] and [9]. Nevertheless this paper adheres to the Lax-Milgram conditions in order to estimate a lower bound of the first eigenfrequency with the help of Korn's constant which depends as well on the geometry as on the material of the stack.*

Now, a lemma is formulated which gives a lower bound for the eigenfrquencies using the Korn's constant.

Lemma 2.3. *Let Ω be the stack occupied domain with height and width equal to $5mm$ (see section 4) and let the stack be made of PZT-4 ceramic material. Then $590Hz$ is a lower bound for the critical frequency (first resonance).*

Proof. By inserting the ratio of height and width of the actuator into the estimates derived by Ryzhak [18], one obtains that Korn's constant is between 4 and 4.099. The mass density of PZT-4 is $7500\frac{\text{kg}}{\text{m}^3}$ and the smallest eigenvalue of $\underline{\underline{\boldsymbol{C}}}$ is given by 25.6GPa. Thus one obtains, that

$$\begin{aligned} 4.099 \cdot 25.6\text{GPa} &\geq 7500\frac{\text{kg}}{m^3}\omega^2 \\ 588\text{Hz} &\geq f, \end{aligned}$$

where $\omega = 2\pi f$. □

Indeed the first eigenfrequency is larger than this bound (see section 4). However, for practical purposes (injection units) it is sufficient to know, that the driving frequency is below this bound.

2.2 Simplified 2D-models for piezoelectric stack actuators

Starting from the stationary and the steady oscillating problem, existence and uniqueness of weak solutions can be shown also for the simplified models below (see [6, 7]).

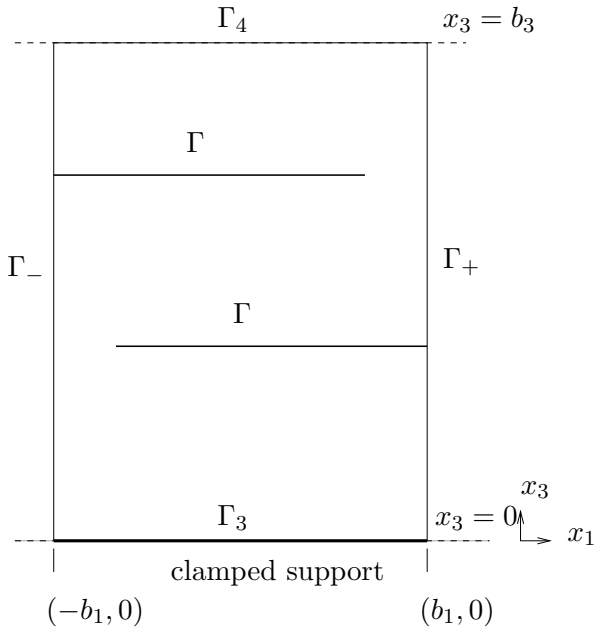

Γ_- $x_1 = -b_1$, $0 \leq x_3 \leq b_3$

Γ_+ $x_1 = +b_1$, $0 \leq x_3 \leq b_3$

Γ_3 $-b_1 \leq x_1 \leq b_1$, $x_3 = 0$,

Γ_4 $-b_1 \leq x_1 \leq b_1$, $x_3 = b_3$

Figure 3: Boundaries and interfaces of a simplified stack actuator model of width $2b_1$, measured in x_1-direction and height b_3.

Due to the small relative thickness $\frac{h_M}{h_C}$ of electrode and ceramic layers, the FE-mesh has to be very fine in order to resolve the discrete solution (see figure 4) which leads to large linear equation systems. Introducing a local coordinate system $x_3 = \epsilon\xi$ at each electrode, we can apply asymptotic methods with respect to the small parameter $\epsilon \approx \frac{h_M}{h_C}$ to reduce the former multi-structure-multi-field problem in Ω to a multi-field problem in a pure ceramic domain $\tilde{\Omega}_C = \Omega \backslash \Gamma$ (here Γ denotes the set of middle lines of the electrodes, see figure 3), where the effect of the electrodes is taken into account by introducing non-standard transmission

conditions on the middle lines of the electrodes. $\underline{\boldsymbol{U}}_C$ is approximated by restricting the solution of the auxiliary problem $\underline{\tilde{\boldsymbol{U}}}_C$ to Ω_C [7].

Stationary model Following the notation in section 2.1 and figure 3, the so called first limit problem reads: Find the displacement $\underline{\tilde{\boldsymbol{u}}}_C(\underline{\boldsymbol{x}})$ and the electric potential field $\tilde{\Phi}_C(\underline{\boldsymbol{x}})$ such that:

System of partial differential equations

$$-\mathcal{D}^\top \underline{\underline{\boldsymbol{C}}}_C \mathcal{D}\underline{\tilde{\boldsymbol{u}}}_C - \mathcal{D}^\top \underline{\underline{\boldsymbol{e}}}^\top \nabla\tilde{\Phi}_C = \underline{\mathbf{0}} \qquad \text{in } \tilde{\Omega}_C, \tag{2.47}$$

$$-\operatorname{div}\left(-\underline{\underline{\boldsymbol{e}}}\,\mathcal{D}\underline{\tilde{\boldsymbol{u}}}_C + \underline{\underline{\boldsymbol{\varepsilon}}}\,\nabla\tilde{\Phi}_C\right) = 0 \qquad \text{in } \tilde{\Omega}_C. \tag{2.48}$$

Boundary conditions

$$\boldsymbol{\sigma}_{C_n}\left(\underline{\tilde{\boldsymbol{u}}}_C, \tilde{\Phi}_C\right) = \underline{\mathbf{0}} \qquad \text{on } (\Gamma_\mp \cup \Gamma_4) \cap \partial\tilde{\Omega}_C, \tag{2.49}$$

$$\tilde{\Phi}_C = \mp\Phi_a \qquad \text{on } \Gamma_\mp \cup \Gamma, \tag{2.50}$$

$$\underline{\tilde{\boldsymbol{u}}}_C = \underline{\mathbf{0}} \qquad \text{on } \Gamma_3, \tag{2.51}$$

$$D_{C_n}\left(\underline{\tilde{\boldsymbol{u}}}_C, \tilde{\Phi}_C\right) = 0 \qquad \text{on } (\Gamma_3 \cup \Gamma_4) \cap \partial\tilde{\Omega}_C, \tag{2.52}$$

where Φ_a is constant.

Transmission conditions

$$[\boldsymbol{\sigma}_{C_n}\left(\underline{\tilde{\boldsymbol{u}}}_C, \tilde{\Phi}_C\right)] = \underline{\mathbf{0}} \qquad \text{on } \Gamma, \tag{2.53}$$

$$[\underline{\tilde{\boldsymbol{u}}}_C] = \underline{\mathbf{0}} \qquad \text{on } \Gamma. \tag{2.54}$$

$\left[\underline{\boldsymbol{f}}\right]$ denotes the jump of a vector-valued function $\underline{\boldsymbol{f}}$ on Γ.
Then the weak solutions $\underline{\tilde{\boldsymbol{U}}}^0_C = \begin{pmatrix} \underline{\tilde{\boldsymbol{u}}}^0_C \\ \tilde{\Phi}^0_C \end{pmatrix}$ (homogeneous Dirichlet data) are sought in the space $\tilde{\mathcal{V}}$, where

$$\tilde{\mathcal{V}} := \left\{ \underline{\tilde{\boldsymbol{V}}} = \begin{pmatrix} \underline{\tilde{\boldsymbol{v}}} \\ \tilde{\Psi} \end{pmatrix} \in \left[\mathsf{H}^1\left(\tilde{\Omega}_C\right)\right]^3, r_{\big|\Gamma_3}\underline{\tilde{\boldsymbol{v}}} = \underline{\mathbf{0}}, \text{ and } r_{\big|\Gamma\cup\Gamma_\pm}\tilde{\Psi} = 0 \right\}.$$

$\underline{\tilde{\boldsymbol{U}}}^0_C$ is found by introducing a smooth continuation $\underline{\tilde{\boldsymbol{W}}} \in \left[\mathsf{H}^1(\Omega)\right]^3$ of the non-homogeneous electrical Dirichlet data on $\Gamma \cup \Gamma_\pm$, such that $\underline{\tilde{\boldsymbol{U}}}_C = \underline{\tilde{\boldsymbol{U}}}^0_C + \underline{\tilde{\boldsymbol{W}}}$.

Lemma 2.4. *Let $\underline{\tilde{\boldsymbol{W}}} \in \left[\mathsf{H}^1\left(\tilde{\Omega}\right)\right]^3$ be a smooth continuation of the non-homogeneous Dirichlet data (2.50) of $\underline{\tilde{\boldsymbol{U}}}_C$ and $\underline{\tilde{\boldsymbol{U}}}^0_C \in \tilde{\mathcal{V}}$ such that $\underline{\tilde{\boldsymbol{U}}}^0_C := \underline{\tilde{\boldsymbol{U}}}_C - \underline{\tilde{\boldsymbol{W}}}$ Then for every $\underline{\tilde{\boldsymbol{V}}} \in \tilde{\mathcal{V}}$, the weak formulation of the boundary-transmission problem (2.47)-(2.54) reads:*
Find $\underline{\tilde{\boldsymbol{U}}}^0_C \in \tilde{\mathcal{V}}$ such that

$$\tilde{a}\left(\underline{\tilde{\boldsymbol{U}}}^0_C, \underline{\tilde{\boldsymbol{V}}}\right) = -\tilde{a}\left(\underline{\boldsymbol{W}}, \underline{\tilde{\boldsymbol{V}}}\right) \tag{2.55}$$

holds for all $\underline{\tilde{\boldsymbol{V}}} \in \tilde{\mathcal{V}}$, where

$$\tilde{a}\left(\underline{\tilde{\boldsymbol{U}}}^0_C, \underline{\tilde{\boldsymbol{V}}}\right) := \int_{\tilde{\Omega}_C} \underline{\underline{\boldsymbol{A}}}_C \underline{\underline{\boldsymbol{B}}}\,\underline{\tilde{\boldsymbol{U}}}^0_C \cdot \underline{\underline{\boldsymbol{B}}}\,\underline{\tilde{\boldsymbol{V}}}\,\mathrm{d}\underline{\boldsymbol{x}}$$

Proof. See [7], section 3.1.1..

a)

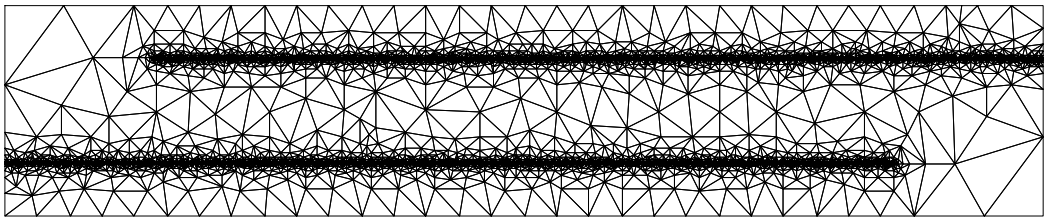

b)

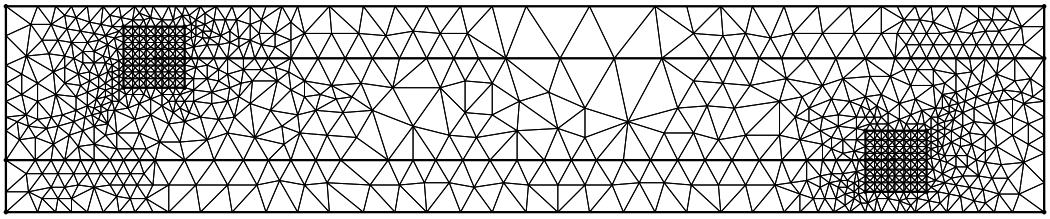

Figure 4: 2D-mesh for one layer of the multi-layer actuator with realistic proportions: a) real electrodes (114874 elements), b) interface conditions instead of electrodes (1827 elements) with angles bigger than 32 in each case.

Steady oscillations (Helmholtz-type model) The simplified formulation for the steady-oscillations case is done analogously to the full one: it is assumed, that $\underline{\tilde{\mathbf{u}}}_C(\underline{\boldsymbol{x}}, t)$ and $\tilde{\Phi}_C(\underline{\boldsymbol{x}}, t)$ are of the form

$$\underline{\tilde{\mathbf{u}}}_C := e^{i\omega t}\underline{\tilde{\boldsymbol{u}}}_C, \quad \tilde{\Phi}_C := e^{i\omega t}\tilde{\Phi}_C.$$

Then the steady-oscillating problem reads: Find the amplitude of the displacement field $\underline{\tilde{\boldsymbol{u}}}_C(\underline{\boldsymbol{x}})$ and the electric potential field $\tilde{\Phi}_C(\underline{\boldsymbol{x}})$, such that:

System of partial differential equations

$$-\rho\omega^2\underline{\tilde{\boldsymbol{u}}}_C - \mathcal{D}^\top\underline{\underline{\boldsymbol{C}}}_C\mathcal{D}\underline{\tilde{\boldsymbol{u}}}_C - \mathcal{D}^\top\underline{\underline{\boldsymbol{e}}}^\top\nabla\tilde{\Phi}_C = \underline{\mathbf{0}} \qquad \text{in } \tilde{\Omega}_C, \tag{2.56}$$

$$-\operatorname{div}\left(-\underline{\underline{\boldsymbol{e}}}\,\mathcal{D}\underline{\tilde{\boldsymbol{u}}}_C + \underline{\underline{\boldsymbol{\varepsilon}}}\,\nabla\tilde{\Phi}_C\right) = 0 \qquad \text{in } \tilde{\Omega}_C. \tag{2.57}$$

Boundary conditions

$$\boldsymbol{\sigma}_{C_n}\left(\underline{\tilde{\boldsymbol{u}}}_C, \tilde{\Phi}_C\right) = \underline{\mathbf{0}} \qquad \text{on } (\Gamma_\mp \cup \Gamma_4) \cap \partial\tilde{\Omega}_C, \tag{2.58}$$

$$\tilde{\Phi}_C = \mp\Phi_a \qquad \text{on } \Gamma_\mp \cup \Gamma, \tag{2.59}$$

$$\underline{\tilde{\boldsymbol{u}}}_C = \underline{\mathbf{0}} \qquad \text{on } \Gamma_3, \tag{2.60}$$

$$D_{C_n}\left(\underline{\tilde{\boldsymbol{u}}}_C, \tilde{\Phi}_C\right) = 0 \qquad \text{on } (\Gamma_3 \cup \Gamma_4) \cap \partial\tilde{\Omega}_C, \tag{2.61}$$

where Φ_a is constant.

In the asymptotic approach, used to deduce this simplified model, the term $\rho\omega^2\underline{\tilde{\boldsymbol{u}}}_C$ does not

contribute to the first order approximation of the transmission conditions, also called *first limit problem* (see [7]). Thus, the transmission conditions are given in standard form.

Transmission conditions

$$[\boldsymbol{\sigma}_{C_n}\left(\underline{\tilde{\boldsymbol{u}}}_C, \tilde{\Phi}_C\right)] = \underline{\mathbf{0}} \qquad \text{on } \Gamma, \tag{2.62}$$

$$[\underline{\tilde{\boldsymbol{u}}}_C] = \underline{\mathbf{0}} \qquad \text{on } \Gamma. \tag{2.63}$$

Lemma 2.5. *Let* $\underline{\boldsymbol{W}} = \begin{pmatrix} \underline{\mathbf{0}} \\ \tilde{\Phi} \end{pmatrix} \in \left[\mathsf{H}^1(\Omega)\right]^3$ *be a smooth continuation of the non-homogeneous Dirichlet data of* $\underline{\tilde{\boldsymbol{U}}}_C$ *and* $\underline{\tilde{\boldsymbol{U}}}^0_C = \begin{pmatrix} \underline{\tilde{\boldsymbol{u}}}^0_C \\ \tilde{\Phi}^0_C \end{pmatrix} := \underline{\tilde{\boldsymbol{U}}}_C - \underline{\boldsymbol{W}}$, *such that* $\underline{\tilde{\boldsymbol{U}}}^0_C, \underline{\tilde{\boldsymbol{V}}} \in \tilde{\mathcal{V}}$. *Then the weak formulation of the boundary-transmission problem (2.56)-(2.63) reads: Find* $\underline{\tilde{\boldsymbol{U}}}^0_C \in \tilde{\mathcal{V}}$ *such that*

$$\tilde{a}_{so}\left(\underline{\tilde{\boldsymbol{U}}}^0_C, \underline{\tilde{\boldsymbol{V}}}\right) = -\tilde{a}_{so}\left(\underline{\boldsymbol{W}}, \underline{\tilde{\boldsymbol{V}}}\right) \tag{2.64}$$

holds for all $\underline{\tilde{\boldsymbol{V}}} \in \tilde{\mathcal{V}}$, *where*

$$\tilde{a}_{so}\left(\underline{\tilde{\boldsymbol{U}}}^0_C, \underline{\tilde{\boldsymbol{V}}}\right) := -\rho\omega^2 \int_{\tilde{\Omega}_C} \underline{\tilde{\boldsymbol{u}}}_C \cdot \underline{\tilde{\boldsymbol{v}}}_C \, \mathrm{d}\underline{\boldsymbol{x}} + \int_{\tilde{\Omega}_C} \underline{\underline{\boldsymbol{A}}}_C \underline{\underline{\boldsymbol{B}}} \underline{\tilde{\boldsymbol{U}}}^0_C \cdot \underline{\underline{\boldsymbol{B}}} \underline{\tilde{\boldsymbol{V}}} \, \mathrm{d}\underline{\boldsymbol{x}}. \tag{2.65}$$

Proof. Inserting the boundary and transmission conditions (2.58)-(2.63) and substituting Ω by $\tilde{\Omega}_C$, $\underline{\boldsymbol{U}}$ by $\underline{\tilde{\boldsymbol{U}}}_C$ and $\underline{\boldsymbol{V}}$ by $\underline{\tilde{\boldsymbol{V}}}_C$, the proof is analogously to the proof of lemma 2.2. □

3 Regularity and finite element error estimates

The numerical simulations, based on the weak formulations in section 2 are computed in conforming discrete subspaces $\mathcal{V}_h \subset \mathcal{V}$ and $\tilde{\mathcal{V}}_h \subset \tilde{\mathcal{V}}$. Therefore, the existence and uniqueness results (Lax-Milgram conditions) also hold for the discretised models. Since the following considerations hold in both cases, $\tilde{\mathcal{V}}$ and $\mathcal{V}$, the formulation will be kept in the space $\mathcal{V}$ for shortness reasons.
Let $\{\underline{\boldsymbol{V}}_1, \ldots, \underline{\boldsymbol{V}}_n\}$ be the basis of the finite-dimensional subspaces $\mathcal{V}_h$, where the basis elements $\underline{\boldsymbol{V}}_i$ are piecewise linear. The Galerkin equations

$$a\left(\underline{\boldsymbol{U}}_h, \underline{\boldsymbol{V}}_k\right) = a\left(\underline{\boldsymbol{W}}, \underline{\boldsymbol{V}}_k\right) \quad k = 1, \ldots, n$$

lead to a linear equation with the discrete solution $\underline{\boldsymbol{U}}_h = \sum_{i=1}^n \alpha_i \underline{\boldsymbol{V}}_i$. The difference in the $\|\cdot\|_{\mathcal{V}}$-norm between the solution $\underline{\boldsymbol{U}}$ and the discrete solution $\underline{\boldsymbol{U}}_h$ can be estimated as follows:

Theorem 3.1 (Cea's Lemma). *Let* a *be the* $\mathcal{V}$*-elliptic, continuous bilinear form (2.29) and* $\mathfrak{A}$ *the corresponding operator. Furthermore let* $\underline{\boldsymbol{U}}_h \in \mathcal{V}_h$. *Then the following estimate holds*

$$\|\underline{\boldsymbol{U}} - \underline{\boldsymbol{U}}_h\|_{\mathcal{V}} \leq \frac{C}{\alpha} \min_{\underline{\boldsymbol{V}} \in \mathcal{V}_h} \|\underline{\boldsymbol{U}} - \underline{\boldsymbol{V}}\|_{\mathcal{V}}$$

with the ellipticity constant α *and the continuity constant* C.

Proof. It holds for all $\underline{\boldsymbol{V}} \in \mathcal{V}_h$ (weak formulation):

$$\begin{aligned}\langle \mathfrak{A}\underline{\boldsymbol{U}}\,, \underline{\boldsymbol{V}}\,\rangle &= \langle\, \underline{\boldsymbol{f}}\,, \underline{\boldsymbol{V}}\,\rangle \\ \langle \mathfrak{A}\underline{\boldsymbol{U}}_h, \underline{\boldsymbol{V}}\,\rangle &= \langle\, \underline{\boldsymbol{f}}\,, \underline{\boldsymbol{V}}\,\rangle\end{aligned}$$

and thus

$$\langle\, \mathfrak{A}\,(\underline{\boldsymbol{U}}_h - \underline{\boldsymbol{U}}\,)\,, \underline{\boldsymbol{V}}\,\rangle = 0 \quad \forall \underline{\boldsymbol{V}} \in \mathcal{V}_h.$$

Since $\underline{\boldsymbol{U}}_h - \underline{\boldsymbol{V}} \in \mathcal{V}_h$ for arbitrary $\underline{\boldsymbol{V}} \in \mathcal{V}_h$, we have

$$\begin{aligned}\|\underline{\boldsymbol{U}}_h - \underline{\boldsymbol{U}}\,\|_{\mathcal{V}}^2 &\leq \frac{1}{\alpha} a\,(\underline{\boldsymbol{U}}_h - \underline{\boldsymbol{U}}\,, \underline{\boldsymbol{U}}_h - \underline{\boldsymbol{U}}\,) \\ &= \frac{1}{\alpha} a\,(\underline{\boldsymbol{U}}_h - \underline{\boldsymbol{U}}\,, \underline{\boldsymbol{U}}_h - \underline{\boldsymbol{V}}\,) + a\,(\underline{\boldsymbol{U}}_h - \underline{\boldsymbol{U}}\,, \underline{\boldsymbol{V}} - \underline{\boldsymbol{U}}\,) \\ &\leq \frac{C}{\alpha}\,\|\underline{\boldsymbol{U}}_h - \underline{\boldsymbol{U}}\,\|_{\mathcal{V}}\,\|\underline{\boldsymbol{U}} - \underline{\boldsymbol{V}}\,\|_{\mathcal{V}}\,.\end{aligned}$$

If $\|\underline{\boldsymbol{U}}_h - \underline{\boldsymbol{U}}\,\| = 0$, the inequality holds trivially. Thus with $\|\underline{\boldsymbol{U}}_h - \underline{\boldsymbol{U}}\,\| \neq 0$, we can divide by $\|\underline{\boldsymbol{U}}_h - \underline{\boldsymbol{U}}\,\|$ to obtain

$$\begin{aligned}\|\underline{\boldsymbol{U}}_h - \underline{\boldsymbol{U}}\,\|_{\mathcal{V}} &\leq \frac{C}{\alpha}\,\|\underline{\boldsymbol{U}} - \underline{\boldsymbol{V}}\,\|_{\mathcal{V}} \quad \forall \underline{\boldsymbol{V}} \in \mathcal{V}_h \\ &\leq \min_{\underline{\boldsymbol{V}} \in \mathcal{V}_h} \frac{C}{\alpha}\,\|\underline{\boldsymbol{U}} - \underline{\boldsymbol{V}}\,\|_{\mathcal{V}}\,.\end{aligned}$$

□

The above estimate in Cea's lemma holds at least in the space $\mathcal{V} \subset \mathsf{H}^1(\Omega) = W_2^1(\Omega)$. The regularity theory for elliptic boundary-transmission problems [8, 16, 13] admits better estimates which can be obtained by splitting $\underline{\boldsymbol{U}} \in \mathcal{V} \subset W_2^1(\Omega)$ into a smooth and a singular part. This is done by multiplying $\underline{\boldsymbol{U}}$ with a cut-off function η with $\mathrm{supp}\,(\eta) \subset \mathcal{E}$, where $\mathcal{E}$ is a neighbourhood of a critical point. By introducing polar coordinates (r, θ) within $\mathcal{E}$, $\underline{\boldsymbol{U}}$ can be written as a power series in r such that

$$\begin{aligned}\eta\underline{\boldsymbol{U}} &= \eta\underline{\boldsymbol{U}}_{reg} + \eta\underline{\boldsymbol{U}}_{sing} \\ \underline{\boldsymbol{U}}_{sing} &= \sum_{\mathrm{Re}\,\alpha \in (0,1)} r^{\alpha}\underline{\boldsymbol{G}}_{\alpha}\,(\ln r, \theta)\end{aligned}$$

with $\underline{\boldsymbol{U}}_{reg} \in W_2^2(\Omega)$ and $\underline{\boldsymbol{G}}_{\alpha}$ smooth. The corresponding local homogeneous partial differential equation system reduces in polar coordinates to an ordinary differential equation system which depends quadratically on the exponent α. By a 1D-FEM Ansatz with respect to the polar angle θ, one obtains a quadratic eigenvalue problem for α, where $(\alpha, \underline{\boldsymbol{G}}_{\alpha})$ are determined as corresponding eigenpairs [5]. Here, numerical approximations yield $\alpha = \frac{1}{2}$ (simplified model) and $\alpha = 0.58$ (full model, dependent on the material parameters, here: PZT 4 and AgPd) for the smallest positive eigenvalue α (leading singularities). In consequence, $\underline{\tilde{\boldsymbol{U}}} \in W_2^{\frac{3}{2}-\epsilon}\left(\tilde{\Omega}\right)$ and $\underline{\boldsymbol{U}} \in W_2^{1.58-\epsilon}(\Omega)$, which will be used in the now following error estimate (3.1) for finite element approximations. Note, that for other geometries, the singularities are different.
A finite element is defined as [3, 2]

Definition 3.1 ([2], 3.1.1). *Let*

- $K \subseteq \mathbb{R}^n$ *be a domain with piecewise smooth boundary (element domain)*
- $\mathcal{P}$ *be a finite-dimensional space of functions on* K *(shape functions)*
- $\mathcal{N} = \{N_1, N_2, \ldots, N_k\}$ *be a basis for the dual* $\mathcal{P}'$ *of* $\mathcal{P}$ *(nodal variables).*

Then $(K, \mathcal{P}, \mathcal{N})$ *is called a finite element.*

The local interpolant is given by the following

Definition 3.2 ([2], 3.3.1). *Given a finite element* $(K, \mathcal{P}, \mathcal{N})$*, let the set* $\{\phi_i : 1 \leq i \leq d\} \subseteq \mathcal{P}$ *be the dual to* $\mathcal{N}$*. If* $\underline{\boldsymbol{V}}$ *is a function for which all* $N_i \in \mathcal{N}$ *are defined, then we define the local interpolant by*

$$\mathcal{I}_K \underline{\boldsymbol{V}} := \sum_{i=1}^{d} N_i(\underline{\boldsymbol{V}})\phi_i.$$

In this setting, the following theorem (see 4.4.20 [2]) for the finite element error estimate holds:

Theorem 3.2. *Let* $\{\mathcal{T}^h\}$ *be a quasi-uniform triangulation of the domain* Ω *and let* $(K, \mathcal{P}, \mathcal{N})$ *be a linear Lagrange reference element. For all* $T \in \mathcal{T}^h$ *let* $(T, \mathcal{P}_T, \mathcal{N}_T)$ *be the affine-equivalent element. Then there exists a positive constant* c *depending on the reference element,* m*,* p *and the radius* ρ *of the largest ball, contained in* T *such that for* $1 \leq s$*,*

$$\begin{aligned}\left(\sum_{T\in\mathcal{T}^h} \left\|\underline{\boldsymbol{V}} - \mathcal{I}^h\underline{\boldsymbol{V}}\right\|^2_{W_2^1(T)}\right)^{\frac{1}{2}} &\leq ch^{s-1}\left|\underline{\boldsymbol{V}}\right|_{W_2^s(\Omega)}, \quad \forall \underline{\boldsymbol{V}} \in W_2^1(\Omega) \\ &\leq ch^{s-1}\left\|\underline{\boldsymbol{V}}\right\|_{W_2^s(\Omega)}, \end{aligned} \tag{3.1}$$

where $\mathcal{I}^h$ *is the global interpolation operator*

$$\mathcal{I}^h\underline{\boldsymbol{U}}\, r\big|_T := \mathcal{I}_T^h\underline{\boldsymbol{U}} \quad \text{for } T \in \mathcal{T}^h.$$

To compare the theoretically predicted error with the numerical result, one usually constructs a solution, computes the right hand sides and uses this data for the numerical simulation to obtain the difference between the discrete solution and the given one, e.g. in the H^1-norm. Finding such a solution in this case is not trivial. Therefore it is assumed that the solution to the finest discretisation level should play the role of a given solution $\underline{\boldsymbol{U}}$ here in the asymptotic model, which is compared with the solutions on the coarse grids. From the fourth refinement level on ($h \approx 1.0^{-4}$), the convergence rates in the above example of figure 5, which should be of order $h^{\frac{1}{2}}$ grow from order $h^{0.1}$ up to $h^{0.3}$.

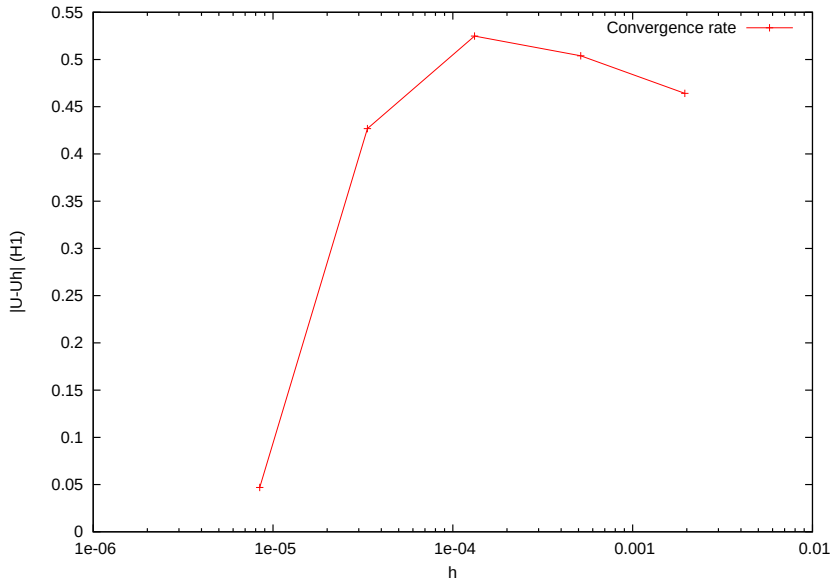

Figure 5: Interface model (see section 4). H^1-Error over h (logarithmic scale).

4 Numerical results

Based on the weak formulations introduced in (2.29),(2.42),(2.55) and (2.64), the finite element approach results in a skew-symmetric linear equation system, which corresponds to the block-structure of $\underline{\underline{\boldsymbol{A}}}$.
The meshes for the finite element approximation were generated with triangle [20, 21], the simulation was done with the C++-library MyFEM++ [15] and it was visualised using the VTK-Library [12, 11, 19].
To assure convergence, the material parameters which range from 10^{10} to 10^{-12} were rescaled and the MyFEM++ -library was extended by a solver for the corresponding Schur-complement system and a Bramble Pasciack Conjugated Gradient solver (BPCG), which is described in [22]. The latter showed to be most effective with respect to iterations and time.
The computations in this section have been done for Barium-Titanate [4]. In the first part, the stationary problem is simulated for different geometries, included the limit case of electrodes with thickness zero. The second part deals with the steady-oscillation case for the full and the interface problem under the influence of the exciting frequency ω.
At the end of each subsection, a short review of the numerical results will be given.

4.1 Stationary case for the model problems

The following computations have been done for a brittle ceramic material: Barium-Titanate. Beginning from the first example the ratio of electrode length and height has been augmented in every example step, this means, that the electrode gets longer and thinner up to the limit case of height (thickness) 0.
The meshing of the stack was processed by Triangle [20, 21] with a required minimal angle of 32° in each triangle. All computations were run on a Intel Pentium IV (3.2GHz) machine.

Example 1 Full 2D-model with thick electrodes.

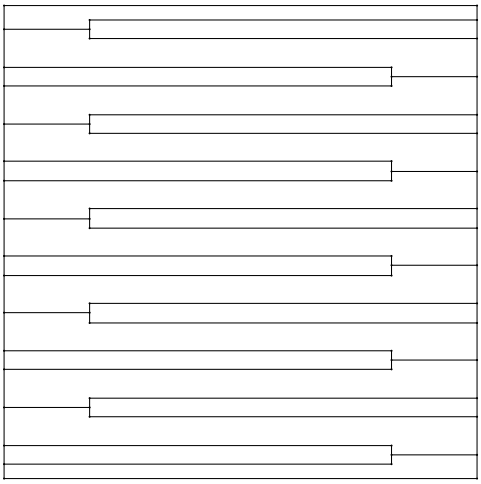

	Barium-Titanate
width [mm]	5
height [mm]	5
electrode length	4.1
electrode height	0.2
iterations	1205
nodes	75857
potential [kV]	[-0.217,0.214]
stroke [mm]	0.000530

Electric potential

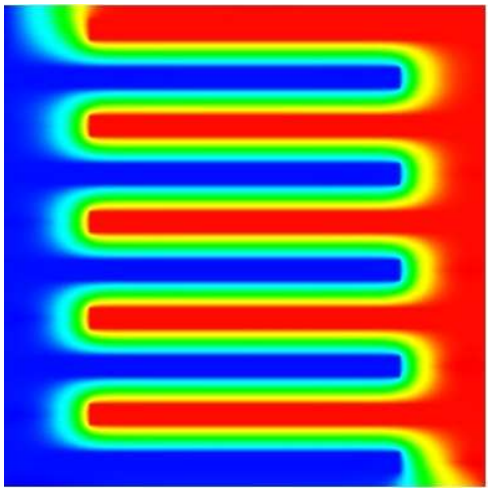

Displacement magnitude

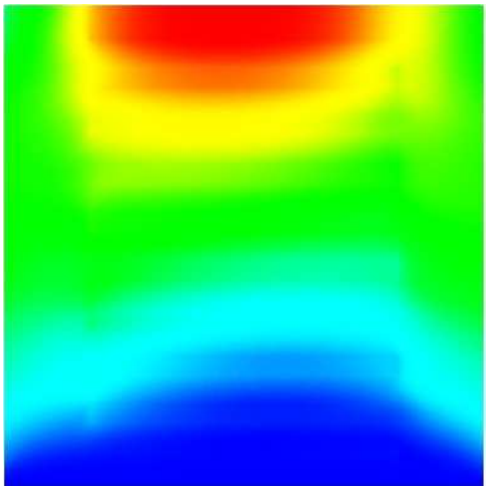

Electric vector field magnitude

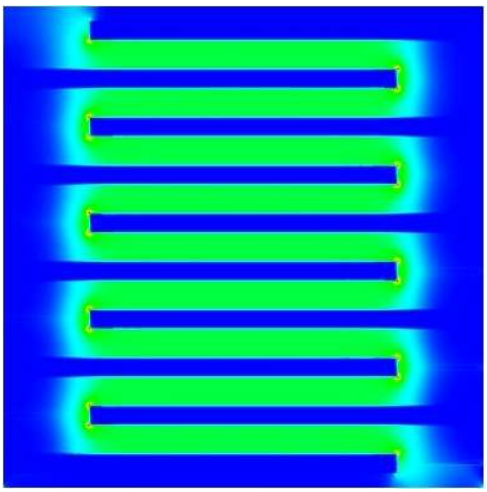

Stress magnitude

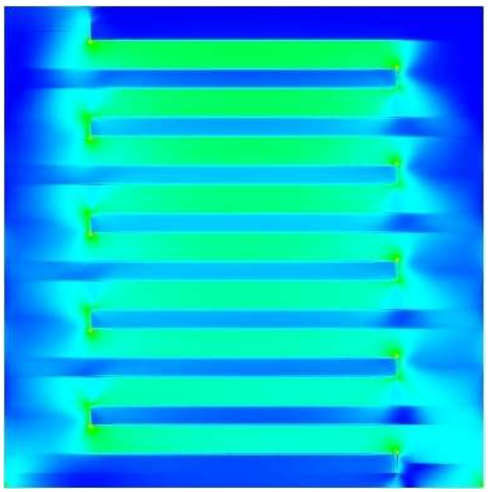

Example 2 Full 2D-model with thin electrodes.

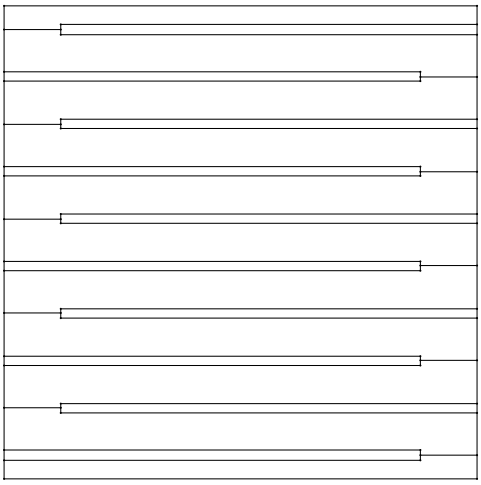

	Barium-Titanate
width [mm]	5
height [mm]	5
electrode length	4.4
electrode height	0.1
iterations	1036
nodes	160453
potential [kV]	[-0.206,0.201]
stroke [mm]	0.000552

Electric potential

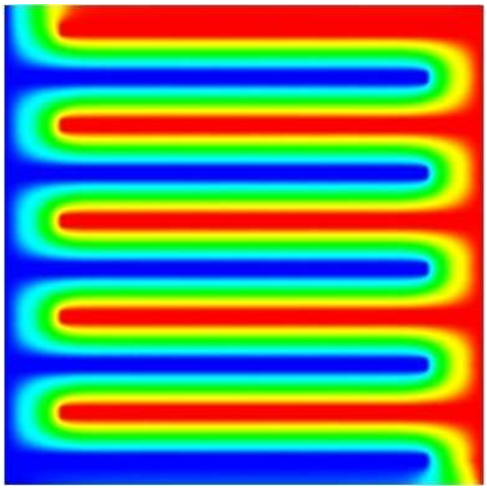

Displacement magnitude

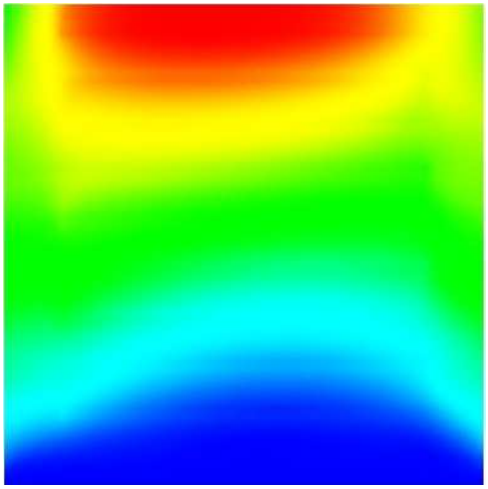

Electric vector field magnitude

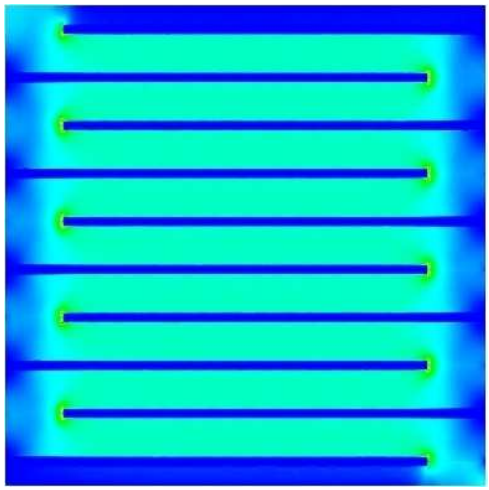

Stress magnitude

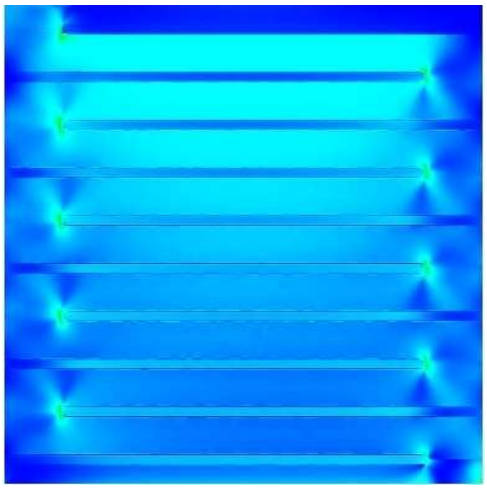

Example 3 Simplified 2D-model with interfaces.

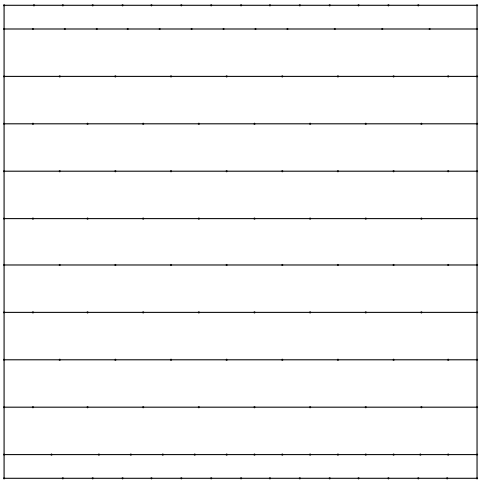

	Barium-Titanate
width [mm]	5
height [mm]	5
electrode length	4.7
electrode height	0
iterations	204
nodes	7569
potential [kV]	[-0.215,0.212]
stroke [mm]	0.000567

Electric potential

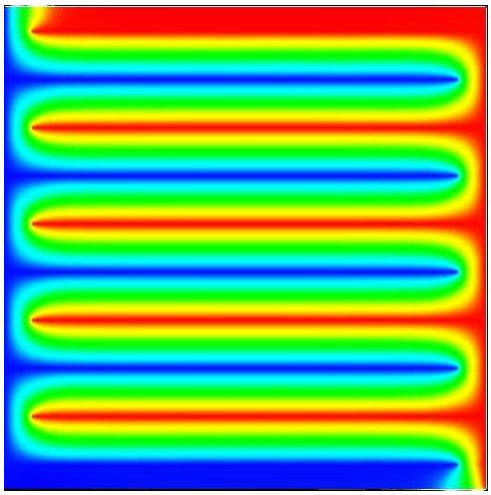

Displacement magnitude

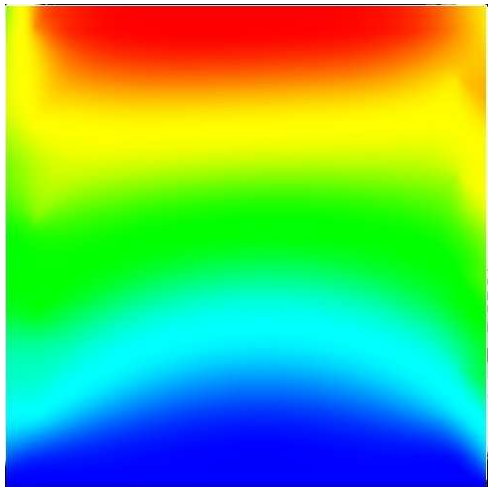

Electric vector field magnitude

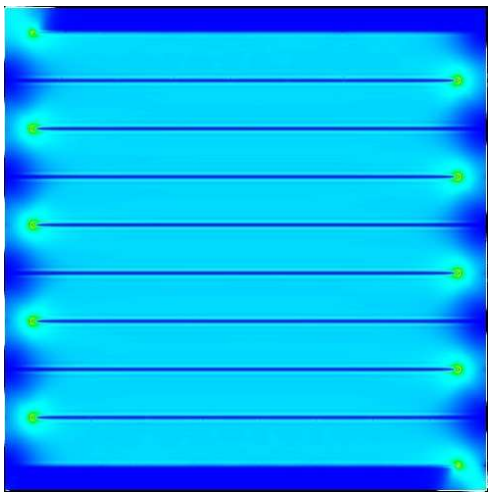

Stress magnitude

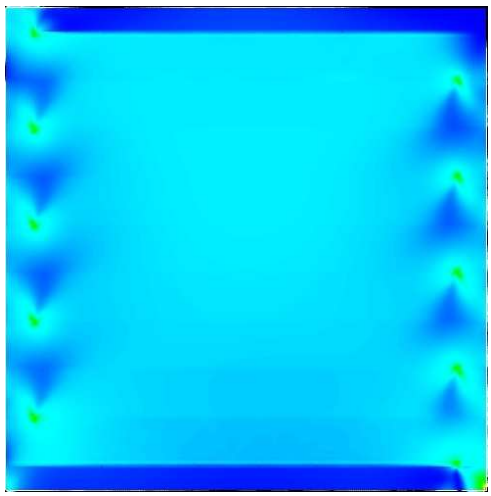

Numerical aspects In the above examples, the mesh has been refined up to a refinement level from which on the relative difference in the H^1-norm between discrete solutions of consecutive refinement levels stayed below the specified computational accuracy. Therefore, the number of nodes varies in the different examples. The thin finger structure of the electrodes, leads to an ill-conditioned system. Especially, in the example 2 with thin electrodes, the number of nodes had to be increased in order to resolve the finger structure. Comparing the values for the stroke, the potential field and the numerical complexity in example 2 with the simplified model in example 3 shows, that the interface-problem provides a good approximation if the electrode is already very thin, while it uses a fractional amount of the computer resources. Since the relation between electrode length and electrode height is even bigger in real-world applications, the interface-model is the right choice particularly for the simulation of stacks with a big number of layers.

Functionality and geometry The influence of the geometrical arrangement and aspect ratio of the electrodes on the functionality of the stack actuator is for direct reading: the larger the active zone (see figure 6) the larger is the stroke of the actuator.

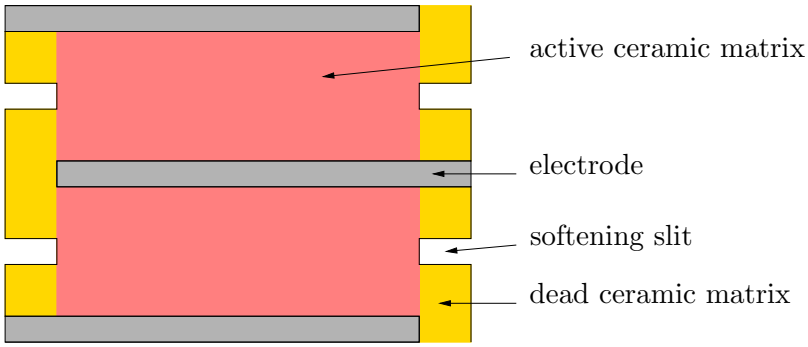

Figure 6: Active and dead zones within a stack actuator with additional slits.

Remark 4.1. *The brittle ceramic material in the outer (dead) zones hinders the stack from growing. To obtain higher growth rates, this material is softened sometimes by inserting small slits (see figure 6).*

Piezoelectric effects triggered by stress singularities From the first glance, it seems irritating, that the range of the computed electric potential Φ is bigger than that of the applied voltage ($[-0.2, 0.2]$kV). To visualise the respective zones, the value ranges are rescaled on the one hand from the lowest value of Φ up to -0.2kV and on the other hand from 0.2kV to the highest value of Φ (see figure 7). Only in the region below the bottom electrode and above the top electrode, the absolute value of Φ exceeds the applied voltage. The explanation is as follows (see figure 7):
The bottom and the top electrode of the stack have no counter electrode. Thus no inverse piezoelectric effect (growth) occurs in those terminal layers. The form in which the constitu-

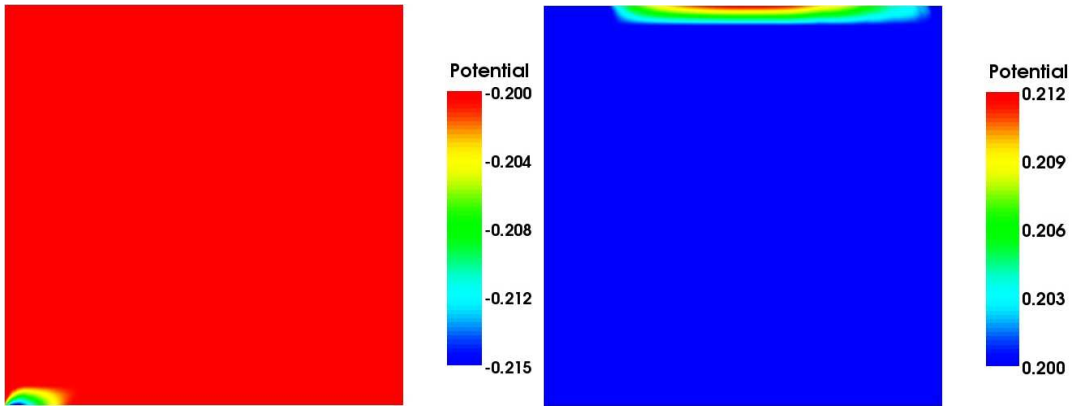

(a) Barium-Titanate

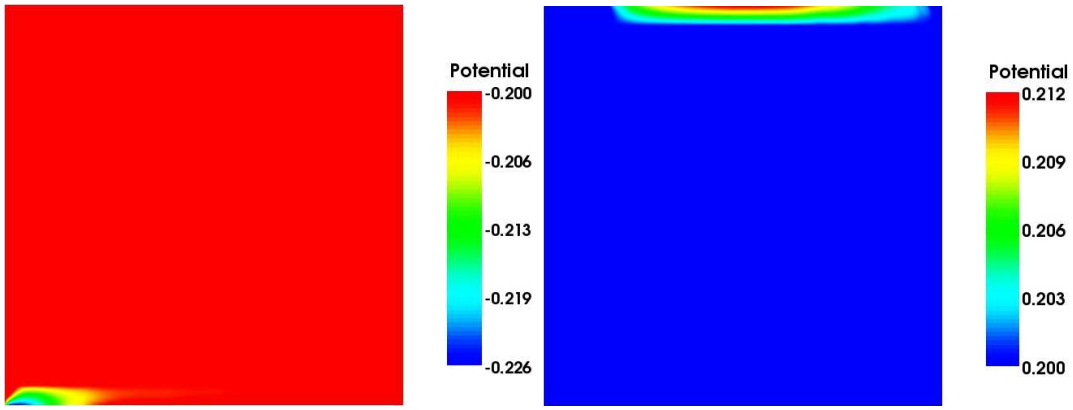

(b) PZT-4

Figure 7: Extremal values of the electric potential field in the corner zones (here: interface problem).

tive equations and thus $\underline{\underline{\boldsymbol{A}}}$ is given is the so called *strain-charge*-form:

$$\begin{pmatrix} \sigma_1 \\ \sigma_3 \\ \sigma_5 \\ D_1 \\ D_3 \end{pmatrix} = \begin{pmatrix} c_{11} & c_{13} & 0 & 0 & -e_{31} \\ c_{13} & c_{33} & 0 & 0 & -e_{33} \\ 0 & 0 & c_{44} & -e_{15} & 0 \\ 0 & 0 & e_{15} & \varepsilon_{11} & 0 \\ e_{31} & e_{31} & 0 & 0 & \varepsilon_{33} \end{pmatrix} \begin{pmatrix} \gamma_1 \\ \gamma_3 \\ \gamma_5 \\ -E_1 \\ -E_3 \end{pmatrix}.$$

The equivalent *strain-voltage*-form reads

$$\begin{pmatrix} \gamma_1 \\ \gamma_3 \\ \gamma_5 \\ -E_1 \\ -E_3 \end{pmatrix} = \begin{pmatrix} f_{11} & f_{13} & 0 & 0 & p_{31} \\ f_{13} & f_{33} & 0 & 0 & p_{33} \\ 0 & 0 & f_{44} & p_{15} & 0 \\ 0 & 0 & p_{15} & -b_{11} & 0 \\ p_{31} & p_{33} & 0 & 0 & -b_{33} \end{pmatrix} \begin{pmatrix} \sigma_1 \\ \sigma_3 \\ \sigma_5 \\ D_1 \\ D_3 \end{pmatrix}, \tag{4.1}$$

where f_{ij} are entries of the elastic compliance tensor, p_{ij} entries of the piezoelectric tensor for the strain-voltage form and b_{ij} entries of the impermeability tensor. Due to the stresses in the corners ($\pm b_1$) of the growing stack, a piezoelectric effect is triggered, which adds due to (4.1) to the potential:

$$-E_1 = p_{15}\sigma_5 - b_{11}D_1 \tag{4.2}$$

$$-E_3 = p_{31}\sigma_1 + p_{33}\sigma_3 \tag{4.3}$$

with $D_3 = 0$ on Γ_3 and Γ_4 due to the boundary conditions. Inserting the material data and the stress components, the red marked terms in (4.2) and (4.3) are dominant and positive in the lowest layer near Γ_3 and negative in the upper layer near Γ_4. Thus the electric potential field falls off in negative x_1- and x_3-direction near Γ_3 and ascends in x_1- and x_3-direction near Γ_4. Since the potential is almost equal to the applied voltages in the regions near the corners, the absolute value of the potential exceeds locally that of the applied voltages.

4.2 Steady oscillations for the simplified stack actuator problem

In section 2.1 a lower bound for the first resonance frequency has already been theoretically determined in the steady oscillation case. The issue of this section is the numerical identification of the first two resonance frequencies of a stack actuator for different ceramic materials. To keep down the numerical costs the stack actuator with interface electrodes, introduced in the previous section has been driven at different frequencies. The following plots show the stroke, dependent on the applied exciting voltage frequency f ($f = 2\pi\omega$) in steps of 50Hz. The stroke is measured in nm.

Eigenfrequencies of the stack (simplified model) The graphs show the stroke for the simplified interface model up to the second resonance for Barium Titanate and PZT-4.

Barium-Titanate

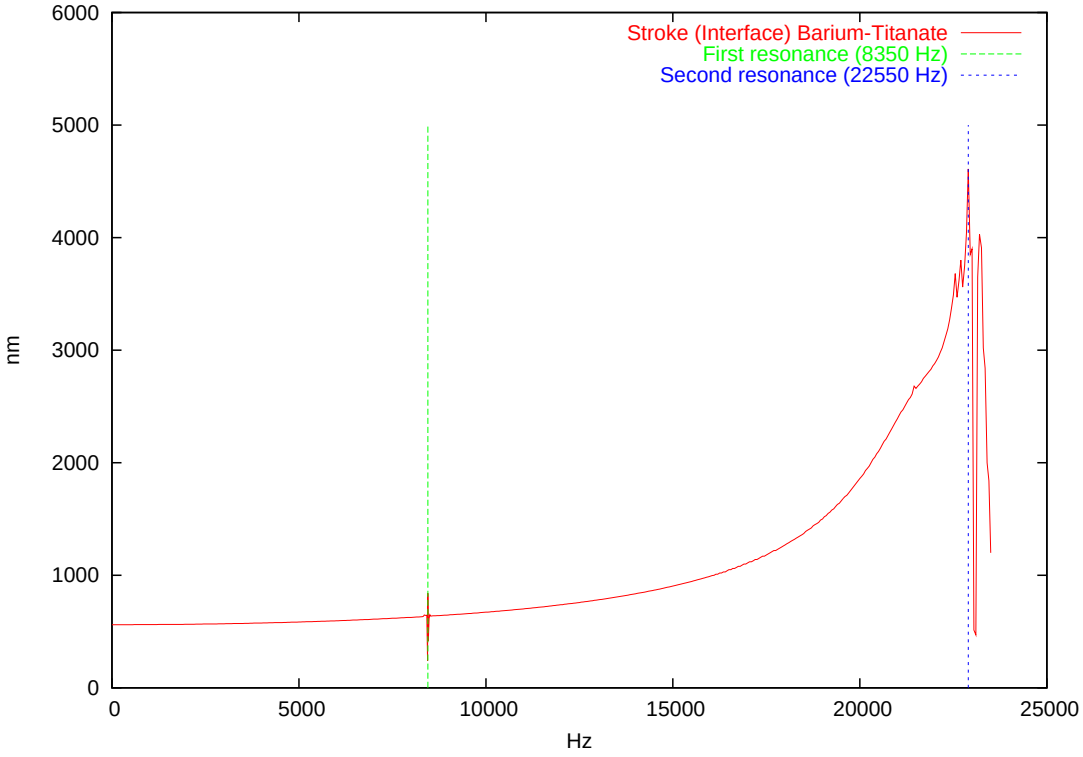

PZT-4

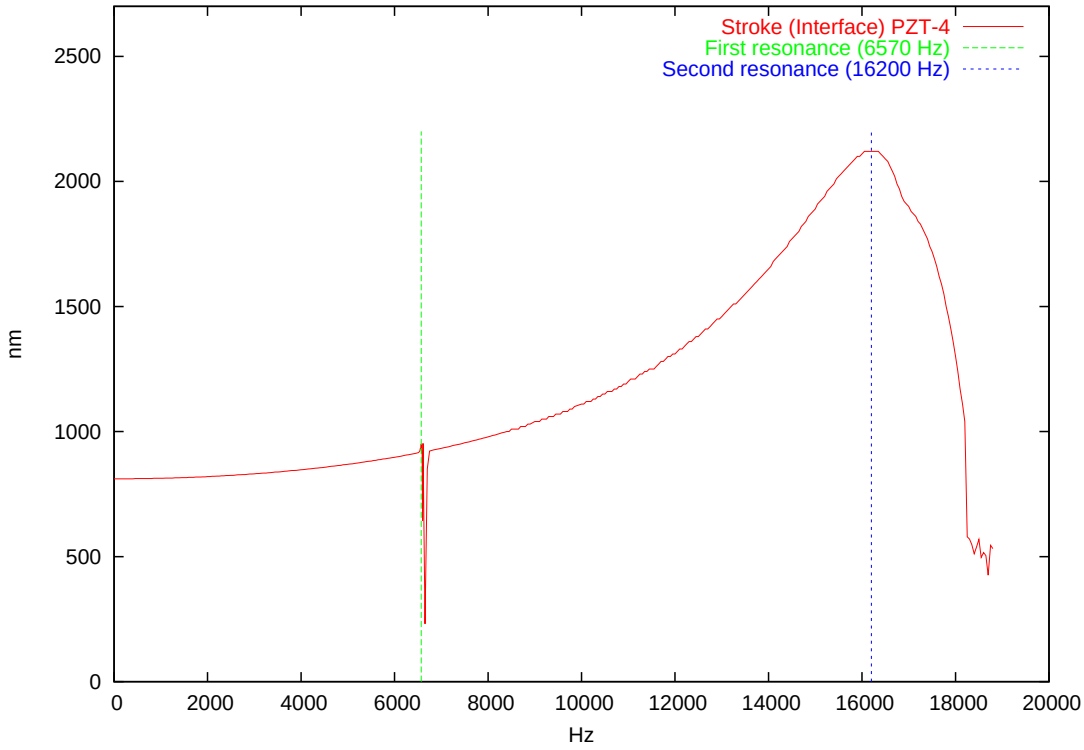

Remarks With this approach it is possible, to determine the resonance frequencies for stack actuators. The peaks especially at the first resonance are high and sharp in either cases. This is due to the fact that the pure Helmholtz type system has been used in the numerical simulation without taking into account additional damping. For applications it is important to drive the actuator at frequencies that are noticeably below the first resonance. With respect to this criterion, the models simulated here satisfy the demands e.g. as injection valves in engines. Due to the small gradient of the graphs below the first resonances, the stationary model which neglects the influence of the exciting frequency can also be used as an approximation for low frequency computations.

References

[1] Braess, D. *Finite Elemente*. Springer Verlag, Berlin Heidelberg, 1997.

[2] Brenner, S. C., and Scott, L. R. *The Mathematical Theory of Finite Element Methods*. Springer Verlag Inc., New York, 1994.

[3] Ciarlet, P. G. *The finite element method for elliptic problems*. SIAM, Philadelphia, 2002.

[4] eFunda, I. eFunda. http://www.efunda.com/.

[5] Geis, W. Determination of stress singularities in piezoelectric stack actuators. *Berichte aus dem Institut für Angewandte Analysis und Numerische Simulation 2005/007* (2005).

[6] Geis, W., Mishuris, G., and Sändig, A.-M. Piezoelectricity in multilayer actuators. Modelling and analysis in two and three dimensions. Preprint 2003/023, University of Stuttgart, http://preprints.ians.uni-stuttgart.de, 2003.

[7] Geis, W., Mishuris, G., and Sändig, A.-M. Asymptotic models for piezoelectric stack actuators with thin metal inclusions. Preprint 2004/001, University of Stuttgart, http://preprints.ians.uni-stuttgart.de, 2004.

[8] Grisvard, P. *Elliptic Problems in Nonsmooth Domains*. Pitman Press, Bath, Avon, 1985.

[9] Kaltenbacher, B., Lahmer, T., and Kaltenbacher, M. PDE based determination of piezoelectric material tensors. Tech. rep., Universität Erlangen, 2005.

[10] Keppeler, S. Common-Rail-Einspritzsystem für den direkteinspritzenden Dieselmotor. Dissertationsschrift, Technische Hochschule, Aachen, 1997.

[11] Kitware, I. ParaView, Version 1.8. http://www.paraview.org/.

[12] Kitware, I. The Visualization Toolkit, Version 4.2. http://www.vtk.org/.

[13] Knees, D. *Regularity results for quasilinear elliptic systems of power-law growth in nonsmooth domains: boundary, transmission and crack problems*. PhD thesis, Universität Stuttgart, 2005. http://elib.uni-stuttgart.de/opus/volltexte/2005/2191/.

[14] Mercier, D., and Nicaise, S. Existence, uniqueness and regularity results for piezoelectric systems. *SIAM Journal on Mathematical Analysis 0* (2005), 000–000.

[15] Merkle, T., and Geis, W. Myfem++, Version 0.0. http://agsaendig.ians.uni-stuttgart.de/MyFEM++.

[16] Nicaise, S., and Sändig, A.-M. General interface problems I. *Mathematical Methods in the Applied Sciences 17* (1994), 327–361.

[17] Qin, Q. H. *Fracture mechanics of piezoelectric materials*. WIT Press, Southampton, Boston, 2001.

[18] Ryzhak, E. Korn's constant for a parallelepiped with a free face or pair of faces. 35–55.

[19] Schroeder, W., Martin, K., and Lorensen, B. *The visualization toolkit: an object-oriented approach to 3D graphics*, 2 ed. Prentice Hall PTR, 1998.

[20] Shewchuk, J. R. Triangle, Version 1.5: A two-dimensional quality mesh generator and delaunay triangulator. http://www-2.cs.cmu.edu/ quake/triangle.html.

[21] Shewchuk, J. R. Triangle: Engineering a 2D Quality Mesh Generator and Delaunay Triangulator. In *Applied Computational Geometry: Towards Geometric Engineering*, M. C. Lin and D. Manocha, Eds., vol. 1148 of *Lecture Notes in Computer Science*. Springer-Verlag, 1996, pp. 203–222.

[22] Steinbach, O. *Numerische Näherungsverfahren für elliptische Randwertprobleme*. Advances in Numerical Mathematics. Teubner Verlagsgesellschaft, 2003.

[23] T. Buchukuri, O. Chkadua, D. N., and Sändig, A.-M. Interaction problems of metallic and piezoelectric materials with regard to thermal stresses. *Berichte aus dem Institut für Angewandte Analysis und Numerische Simulation XX* (200X).

[24] Voigt, W. *Lehrbuch der Kristallphysik*. Teubner-Verlag, Leipzig, 1910.

Winfried Geis
Pfaffenwaldring 57
70569 Stuttgart
Germany
E-Mail: Winfried.Geis@ians.uni-stuttgart.de
WWW: http://ians.uni-stuttgart.de/~geiswd/

Erschienene Preprints ab Nummer 2005/001

Komplette Liste: `http://preprints.ians.uni-stuttgart.de`

2005/001 *S. Nicaise, A.-M. Sändig:* Dynamical crack propagation in a 2D elastic body. The out-of plane state.

2005/002 *S. Hüeber, A. Matei, B.I. Wohlmuth:* A mixed variational formulation and an optimal a priori error estimate for a frictional contact problem in elasto-piezoelectricity

2005/003 *A.-M. Sändig:* Distributionentheorie mit Anwendungen auf partielle Differentialgleichungen. Vorlesung im Wintersemester 2004/2005

2005/004 *A.-M. Sändig, T. Buchukuri, O. Chkadua, D. Natroshvili:* Solvability and regularity results to boundary-transmission problems for metallic and piezoelectric elastic materials

2005/005 *B. Flemisch, B. I. Wohlmuth:* Stable Lagrange multipliers for quadrilateral meshes of curved interfaces in 3D

2005/006 *Geis, W.:* Determination of stress singularities in piezoelectric stack actuators

2005/007 *Geis, W.:* Numerical simulation of linear models for piezoelectric stack actuators